UNCLASSIFIED

DOCUMENTATION PAGE

Form Approved
OMB No. 0704-0188

AD-A207 928 DTIC ELECTE MAY 16 1989 S D

1b. RESTRICTIVE MARKINGS

3. DISTRIBUTION/AVAILABILITY OF REPORT
Approved for Public Release;
Distribution Unlimited.

2b. DECLASSIFICATION/DOWNGRADING SCHEDULE

4. PERFORMING ORGANIZATION REPORT NUMBER(S)
UDR-TR-89-29

5. MONITORING ORGANIZATION REPORT NUMBER(S)
AFOSR-TR- 89-0591

6a. NAME OF PERFORMING ORGANIZATION
University of Dayton
Research Institute

6b. OFFICE SYMBOL (*If applicable*)

7a. NAME OF MONITORING ORGANIZATION
Air Force Office of Scientific Research

6c. ADDRESS (*City, State, and ZIP Code*)
300 College Park
Dayton, OH 45469-0001

7b. ADDRESS (*City, State, and ZIP Code*)
Bolling AFB DC 20332-6448

8a. NAME OF FUNDING/SPONSORING ORGANIZATION
Air Force Office of Scientific Research

8b. OFFICE SYMBOL (*If applicable*)
AFOSR/NM

9. PROCUREMENT INSTRUMENT IDENTIFICATION NUMBER
F-49620-88-C-0040

8c. ADDRESS (*City, State, and ZIP Code*)
Bolling AFB, DC 20332

10. SOURCE OF FUNDING NUMBERS

PROGRAM ELEMENT NO	PROJECT NO	TASK NO	WORK UNIT ACCESSION NO
61102F	2304	A3	

11. TITLE (*Include Security Classification*)
Fast-Algorithm Development for Large-Eddy Simulation of Circular-Jet Turbulence

12. PERSONAL AUTHOR(S)
L. Krishnamurthy

13a. TYPE OF REPORT	13b. TIME COVERED	14. DATE OF REPORT (*Year, Month, Day*)	15. PAGE COUNT
Final	FROM 1/1/1988 TO 12/31/88	1989, March	91

16. SUPPLEMENTARY NOTATION

17. COSATI CODES		
FIELD	GROUP	SUB-GROUP

18. SUBJECT TERMS (*Continue on reverse if necessary and identify by block number*)
Asymptotic Structure, Large-Eddy Simulation, Turbulence Modeling, Farfield Development, Round Jet, Free Jet, Subgrid-Scale Turbulence

19. ABSTRACT (*Continue on reverse if necessary and identify by block number*)

The research reported herein addresses a theoretical investigation of a free, turbulent round jet issuing into a quiescent ambient, and deals with asymptotic analysis for farfield development and subgrid-scale turbulence modeling and with computational considerations for large-eddy simulation. Higher-order asymptotic analysis of the fully developed downstream region has uncovered new information for the stress- and pressure-function solutions in the exterior region. The analytical predictions of the centerline deacy of the mean axial velocity and those of the radial distributions of the axial and radial mean-velocity components and the shear- and normal-stress components compare well with available experimental data and provide the needed farfield boundary conditions for the large-eddy computations. The numerical considerations for the latter examine the construction of hybrid-difference methods that preserve weak but persistent unsteady features, the two-dimensional jet, and dual-variable algorithm for simulating incompressible three-dimensional flows.

20. DISTRIBUTION/AVAILABILITY OF ABSTRACT
☒ UNCLASSIFIED/UNLIMITED ☐ SAME AS RPT ☐ DTIC USERS

21. ABSTRACT SECURITY CLASSIFICATION
Unclassified

22a. NAME OF RESPONSIBLE INDIVIDUAL
Major James M. Crowley

22b. TELEPHONE (*Include Area Code*)
(202)767-4940

22c. OFFICE SYMBOL
AFOSR/NM

DD Form 1473, JUN 86 *Previous editions are obsolete.*

SECURITY CLASSIFICATION OF THIS PAGE
UNCLASSIFIED

89

UDR-TR-89-29

FAST-ALGORITHM DEVELOPMENT FOR LARGE-EDDY SIMULATION OF CIRCULAR-JET TURBULENCE

L. Krishnamurthy

FINAL TECHNICAL REPORT

FOR THE PERIOD 1 JANUARY 1988 THROUGH 31 DECEMBER 1988

AIR FORCE OFFICE OF SCIENTIFIC RESEARCH
CONTRACT NO. F49620-88-C-0040

MARCH 1989

APPROVED FOR PUBLIC RELEASE; DISTRIBUTION UNLIMITED

UNIVERSITY OF DAYTON
RESEARCH INSTITUTE
DAYTON, OHIO 45469-0001

TABLE OF CONTENTS

SECTION I

INTRODUCTION

This final technical report documents the current status and accomplishments of the research performed by the University of Dayton for the Air Force Office of Scientific Research (AFOSR), Broad Agency Announcement under Contract No. F49620-88-C-0040. The research documented herein was conducted by the University of Dayton Research Institute (UDRI) as the prime contractor, with the University of Pittsburgh, Institute for Computational Mathematics and Applications (ICMA), as its subcontractor. Although this document is issued as the final report for the one-year research performed during the reporting period, the research status and accomplishments represent a continuation of the earlier two-year effort which was supported by the AFOSR Fast Algorithm Initiative under Contract No. F49620-85-C-0137.

1. BACKGROUND

The overall theme of the UDRI-ICMA joint research program is the efficient computation of the development of the free turbulent round jet by the time-dependent Navier-Stokes Equations. As discussed in Krishnamurthy et al. (1987), the only feasible approach for predicting jet turbulence at present involves a combination of (i) the direct computation of the complete equations on a coarsely resolved grid (as dictated by available computing resources) to describe the large-scale motion by means of large-eddy simulation (LES), (ii) accurate modeling of subgrid-scale (SGS) turbulence to describe the small-scale motion that is not explicitly resolved, and (iii) the proper coupling of the SGS turbulence model to the LES computations. It is precisely this three-pronged approach that has governed the conduct of the present research program. Accordingly, this report summarizes the salient aspects of the research at UDRI and ICMA, addressing the aforementioned items.

The LES computations have been based upon the ALgorithms for GAs Equations (ALGAE) computer code, which has been developed by ICMA. Although it was recognized that this procedure did not correspond to a true LES of circular-jet turbulence in view of its two-dimensional formulation, the joint research program accepted ALGAE as a baseline computational procedure that can be refined and optimized for the LES of the round jet through successive modifications. Thus, ICMA has continued to be responsible for the development of the LES numerical algorithms and their efficient implementation on vector computers. UDRI has been responsible for research in SGS turbulence modeling, asymptotic development of the farfield structure, and integration of ICMA computational efforts.

2. SCOPE OF RESEARCH

The research on SGS turbulence modeling has investigated one-point closure models and focused on the eddy-viscosity model to facilitate the incorporation of a variable-viscosity capability in the ALGAE procedure. The specific eddy-viscosity model that was suggested for ICMA application to LES computation is based on the algebraic mixing-length formulation of Launder et al. (1972). A crucial aspect of SGS turbulence is the asymptotic analysis of the farfield. Free- and wall-shear turbulent flows asymptotically attain the so-called fully developed state when the flow becomes self-similar. The recent adverse-pressure-gradient boundary-layer asymptotic analysis of Bush and Krishnamurthy (1987) demonstrated the viability of the mixing-length model. Although the boundary-layer analysis is relevant to the case of ducted-jet flowfields, its results are not directly applicable to the case of a free jet. Therefore, present research has addressed the asymptotic analysis of the fully developed region of the round jet to examine the applicability of the eddy-viscosity model to SGS turbulence. The results of this analysis, given in Bush and Krishnamurthy (1988), suggest that the mixing-length model is indeed a good candidate for round-jet SGS turbulence These results provide, in addition, farfield information, with which the conditions imposed in ALGAE computations on certain artificially introduced pseudo boundaries must be consistent. Appendix A documents the round-jet analysis.

Preliminary ALGAE computations at ICMA failed to reproduce the analytical solution of the two-dimensional inviscid jet. This failure was largely due to inadequate spatial resolution near the jet boundary. Subsequent use of a nonzero and constant value of *molecular* viscosity did compute the qualitative features of the analytical solution of the two-dimensional jet. Further computational testing of the ALGAE code has not addressed the flowfield of the round jet and the incorporation of the *turbulent* viscosity that is specified by the mixing-length model. Other computational aspects addressed by ICMA research include the development of a theory dealing with the construction of hybrid-difference methods, and the description of algorithms for the numerical simulation of three-dimensional flows. These are documented in Appendix B.

3. OUTLINE OF REPORT

A brief discussion of the current status and accomplishments of the research is presented in Section II. Section III lists the documentation from the research sponsored under this program. Section IV shows the research personnel supported by this program.

SECTION II

STATUS OF RESEARCH

The following paragraphs summarize the research progress to date. Detailed descriptions are available in the Appendices.

1. ASYMPTOTIC FARFIELD DEVELOPMENT

As emphasized in Krishnamurthy et al. (1987), the initial SGS turbulence modeling effort has investigated one-point closure models and selected the mixing-length eddy-viscosity model for use in ICMA computations. A computational validation of this model by the ALGAE procedure remains to be carried out. Successful validations by LES calculations of the nearfield should serve to provide benchmark data for comparison with more refined SGS models.

Another criterion for establishing the suitability of the SGS turbulence model is the degree of success in its ability to predict the farfield. This requires the determination of the structure of the turbulent jet far enough downstream of the nozzle exit that there is no residual effect of the initial conditions, and self-similarity of the flow is attained. For this downstream region, an asymptotic analysis of the Reynolds time-averaged equations and complementary boundary conditions, with limit-process expansions developed in the limit of large Reynolds number, has been completed and the uniformly valid flow behavior, from the jet centerline to the ambient farfield, has been determined.

The analysis, shown in Appendix A, reveals the existence far downstream of the nozzle exit, of a turbulent core region, an irrotational exterior region, and a distinguished intermediate region. Appropriate independent and dependent variables for all three regions are identified and the self-similar formulations therein are obtained. The solutions for the turbulent normal

stresses and the mean pressure in the core region are ascertained through the consideration of higher-order approximations of the boundary-value problem, in conjunction with the modeling of the experimental data. The resulting core-region solutions are not uniformly valid at the outer edge of this region. To obtain a uniformly valid description of the jet flow, it is necessary to introduce, in addition to the downstream core region, a downstream exterior region, at the outer edge of which the flow quantities reach their ambient values; and a downstream intermediate region, in which there is a change from a core-region-like flow to an exterior-region-like one.

The farfield aspects of the jet flow are not often discussed in the literature. Landau and Lifshitz (1959) determine "the mean flow in the jet outside the turbulent region," which (roughly) corresponds to the downstream exterior region. Present analysis shows that, to leading order of approximation, the exterior region is a turbulent region: the flow is irrotational, yet there is a convection--pressure-gradient--turbulent-stress balance in both the axial and radial momentum equations. Whereas the resulting mean-velocity solutions are essentially those obtained by Landau and Lifshitz, the exterior-region stress- and pressure-function solutions represent *new* information on the farfield flow behavior.

Although the leading-order solutions for the radial velocity in the core and exterior regions match directly, the corresponding solutions for other flow quantities do not. An examination of the leading-order *and* higher-order solutions in these two regions (but especially those for the core region) suggests the existence of a downstream intermediate region. It is seen that in this region the leading-order solutions of all flow quantities match directly to all of the leading-order core-region solutions (in a nearfield overlap domain) and also match directly to all of the leading-order exterior-region solutions (in a farfield overlap domain).

With the presentation of the pertinent core-, exterior-, and intermediate-region solutions and with the determination of the core-region/intermediate-region matching and of the exterior-

region/intermediate-region matching, the uniformly valid picture of the structure of the self-similar turbulent axisymmetric jet is complete. The analytical predictions of the distributions of the axial/radial velocities and the shear stress in the core region are compared with the experimental data of Wygnanski and Fiedler (1969), with good results. Available experimental results, however, do not extend to the exterior region.

The foregoing validation of the eddy-viscosity model in the farfield development of the jet apart, the asymptotic analysis is also of value in providing the needed farfield information for the LES computations. The specification of the boundary conditions is a key issue in the numerical simulation of the jet by the ALGAE code. Whereas the LES research addresses the development of a jet discharging into an unbounded domain, the ALGAE-based computation requires confined flowfields and artificially introduced pseudo boundaries. The axis of symmetry, of course, is a real boundary and does not pose any difficulty. It is the farfield boundaries (at large radial and axial distances) that cause problems. The asymptotic analysis of the fully developed region provides a means to specify these boundary conditions. The asymptotic farfield solutions do apply to the downstream pseudo boundary, provided it is at least 10 jet diameters downstream of the nozzle exit (experimental evidence suggests that the fully developed region occurs between 10 and 50 jet diameters). These solutions also apply to the radially outward boundary (i.e., the top pseudo boundary where free-slip wall conditions have been imposed in the ALGAE computations), but only at axial distances exceeding 10 jet diameters. Thus, it is essential that the ALGAE-based predictions must be consistent with the asymptotic results for axial distances exceeding 10 jet diameters.

2. COMPUTATIONAL CONSIDERATIONS

ICMA research during the reporting period has considered three major computational topics, a detailed discussion of which is presented in Appendix B.

3. REFERENCES

Bush, W. B. and Krishnamurthy, L. (1987) "Asymptotic Analysis of a Turbulent Boundary Layer in a Strong Adverse Pressure Gradient," UDR-TR-87-35, AFOSR-TR-87-0962.

Bush, W. B. and Krishnamurthy, L. (1988) "Asymptotic Analysis of the Fully Developed Region of an Incompressible, Free, Turbulent Round Jet," UDR-TR-88-86. See Appendix A. To be Submitted for Publication.

Landau, L. D. and Lifshitz, E. M. (1959) *Fluid Mechanics. Course of Theoretical Physics* 6. London: Pergamon Press.

Launder, B. E., Morse, A., Rodi, W., and Spalding, D. B. (1972) "The Prediction of Free Shear Flows - A Comparison of the Performance of Six Turbulence Models," in *Proc. NASA Conf. on Free Shear Flows*, NASA SP-321, 1, 361-426.

Krishnamurthy, L., Hall, C. A. and Porsching, T. A. (1987) "Fast-Algorithm Development for Large-Eddy Simulation of Circular-Jet Turbulence," Final Technical Report, UDR-TR-87-150, AFOSR-TR-88-0091.

Wygnanski, I. and Fiedler, H. (1969) "Some Measurements in the Self-Preserving Jet," *J. Fluid Mech.* **38**, 577-612.

SECTION III

DOCUMENTATION

The following reports were supported in part by this research program:

Bush, W. B. and Krishnamurthy, L. (1988) "Asymptotic Analysis of the Fully Developed Region of an Incompressible, Free, Turbulent Round Jet," UDR-TR-88-86. To be submitted for Publication.

Bush, W. B. and Krishnamurthy, L. (1988) "Asymptotic Analysis of an Equilibrium Turbulent Boundary Layer in a Strong Adverse Pressure Gradient," *AIAA J.*, Under Review.

SECTION IV

RESEARCH PERSONNEL

The following were supported in part by this research project:

- UDRI

  L. Krishnamurthy
  Senior Research Engineer

  W. B. Bush
  Consultant

- ICMA

  C. A. Hall
  Professor of Mathematics

  M. Raymund
  Senior Lecturer

  T. A. Porsching
  Professor of Mathematics

APPENDIX A

ASYMPTOTIC ANALYSIS OF THE FULLY DEVELOPED REGION OF AN INCOMPRESSIBLE, FREE, TURBULENT, ROUND JET

By W. B. BUSH

King, Buck & Associates, Inc., San Diego, CA 92110, USA

AND L. KRISHNAMURTHY

University of Dayton Research Institute, Dayton, OH 45469, USA

ABSTRACT

The structure of the farfield turbulent region of an incompressible free jet developing downstream of an axisymmetric nozzle is studied by means of the Reynolds time-averaged equations. The analysis employs the method of matched asymptotic expansions, with limit-process expansions developed in the limit of large Reynolds number. The analysis reveals the existence, far downstream of the nozzle exit, of a turbulent core region, an irrotational exterior region, and a distinguished intermediate region. Self-similar formulations are sought for all three regions in terms of appropriate independent and dependent variables. The stress- and pressure-function solutions for the exterior region, unlike the mean-velocity solutions, represent new information on the farfield flow behavior. The analytical results of the centerline decay of the mean axial velocity and those of the radial distributions of the axial and radial mean-velocity components and the shear- and normal-stress components are compared with available experimental data.

1. INTRODUCTION

The self-similar turbulent round jet, because it is a relatively simple turbulent shear flow, has been the subject of extensive study, theoretical (see, e.g., Abramovich 1963; Hinze 1975; Townsend 1976; Schlichting 1979), as well as experimental (see, e.g., Reichardt 1941; Hinze & Van der Hegge Zijnen 1949; Wygnanski & Fiedler 1969). From the first study (Tollmien 1926) up to the present, the (classical) theoretical approach has been to concentrate on the leading-order approximation of the boundary-value problem for the downstream core region to determine the solutions for the mean velocity and the turbulent shear stress.

This paper presents a theoretical study of the structure of a turbulent incompressible, isothermal jet issuing from an axisymmetric nozzle. Attention is directed to the flowfield region far enough downstream of the nozzle exit that there is no residual effect of the initial conditions and self-similarity is attained. In particular, by means of a higher-order asymptotic analysis of the Reynolds time-averaged equations and complementary boundary conditions, presented in § 2, the uniformly valid behavior of the flow quantities, from the jet centerline to the ambient farfield, is determined for this downstream self-similar region (see figure 1).

In § 3, through the consideration of higher-order approximations of the boundary-value problem, in conjunction with the modeling of the experimental data, the solutions for the turbulent normal stresses and the mean pressure in the core region are also ascertained. This higher-order analysis establishes that the resulting core-region solutions are not uniformly valid at the outer edge of this region. To obtain a uniformly valid picture of the flowfield, it is necessary to introduce, in addition to the downstream core region, a downstream exterior region, at the outer edge of which the flow quantities attain their ambient values; and a downstream intermediate region, in which the flow changes from a core-region-like flow to an exterior-region-like one.

The farfield aspects of the jet flow are not often discussed in the literature. Landau & Lifshitz (1959) determine the "mean flow in the jet outside the turbulent region," which (roughly) corresponds to the downstream exterior region. In § 5, the appropriate scaling of the variables indicates that, to leading order of approximation, the exterior region is a turbulent region: the flow is irrotational, yet there is a convection--pressure-gradient--turbulent-

AMBIENT

EXTERIOR REGION:

$x_s = \delta X$, $r_s = \delta R$: $\xi = (r_s/x_s) = (R/X)$;

$\Psi = \psi_s$: $U = \delta^2 u_s$, $V = \delta^2 v_s$, $\Omega = \delta^3 \omega_s$,

$P = \delta^4 p_s$, $T = \delta^4 \tau_s$, $M = \delta^4 \mu_s$, $N = \delta^4 \nu_s$.

INTERMEDIATE REGION:

$x_k = \delta X$, $r_k = \delta^{1/2} R$: $\theta = (r_k/x_k) = \delta^{-1/2}(R/X)$;

$\Psi = A_0 x_k + \delta \psi_k$: $U = \delta^2 u_k$, $V = -\delta^{3/2} A_0 r_k^{-1} + \delta^{5/2} v_k$, $\Omega = \delta^{5/2} \omega_k$,

$P = \delta^3 p_k$, $T = \delta^{7/2} \tau_k$, $M = \delta^3 \mu_k$, $N = \delta^3 \nu_k$.

CORE REGION:

$x = \delta X$, $r = R$: $\eta = (r/x) = \delta^{-1}(R/X)$;

$\Psi = \psi$: $U = u$, $V = \delta v$, $\Omega = \omega$,

$P = \delta p$, $T = \delta \tau$, $M = \delta \mu$, $N = \delta \nu$.

JET CENTERLINE

Figure 1. Schematic diagram of the asymptotic structure.

stress balance in both the axial and the radial momentum equations. Whereas the resulting mean-velocity solutions are essentially the ones determined by Landau & Lifshitz, the exterior-region stress- and pressure-function solutions represent new information concerning the farfield behavior of the flow.

Although the leading-order core-region and exterior-region solutions for the radial velocity match directly, the corresponding solutions for the other flow quantities do not. An examination of the leading-order *and* higher-order solutions for these two regions (but especially those for the core region) suggests the existence of the downstream intermediate region, formulated and analyzed in § 4. The leading-order intermediate-region solutions of all flow quantities match directly to all of the leading-order core-region solutions (in a nearfield overlap domain) and also match directly to all of the leading-order exterior-region solutions (in a farfield overlap domain).

With the presentation of the pertinent solutions for the core, exterior, and intermediate regions, and with the determination of the core-region/intermediate-region matching and of the exterior-region/intermediate-region matching, the uniformly valid description of the structure of the self-similar turbulent axisymmetric jet is complete. The analytical predictions of the core-region distributions of the axial and radial velocities and the shear stress are compared in § 6 with the experimental data of Wygnanski & Fiedler, with good results. Available experimental results, however, do not extend to the exterior region, as defined in this paper.

2. EQUATIONS OF MEAN MOTION

Consider the steady flow of the axisymmetric/round fully developed turbulent jet of a homogeneous, incompressible fluid ($\tilde{\rho}$ = const.). Let $X = (\tilde{X}-\tilde{X}_o)/\tilde{B}_j$ and $R = \tilde{R}/\tilde{B}_j$ represent the axial and radial coordinates, with $\tilde{X}$, $\tilde{R}$ = 0 denoting the origin of the jet, $\tilde{B}_j$, the initial jet radius, and $\tilde{X}_o$, the "origin of similarity." The mean velocity components in the axial and radial directions, respectively, are $U = \tilde{U}/\tilde{U}_j$ and $V = \tilde{V}/\tilde{U}_j$, with $\tilde{U}_j$, the reference jet-exit speed; the mean pressure is $P = (\tilde{P}-\tilde{P}_\infty)/\tilde{\rho}\tilde{U}_j^2$, with $\tilde{P}_\infty$ denoting the ambient pressure. The turbulent shear- and normal-stress components are $T = T_{XR} = T_{RX} = -(\tilde{u}'\tilde{v}')/\tilde{U}_j^2$, and $M = T_{XX} = -(\tilde{u}'^2)/\tilde{U}_j^2$ and $N = T_{RR} = -(\tilde{v}'^2)/\tilde{U}_j^2$. In the foregoing, the tilde quantities are dimensional, the primes denote the fluctuating quantities, and the overbars denote time-averaging.

The continuity and momentum equations describing the mean flow are

$$\frac{\partial U}{\partial X} + \frac{1}{R}\frac{\partial (RV)}{\partial R} = 0: \quad U = \frac{1}{R}\frac{\partial \Psi}{\partial R}, \; V = -\frac{1}{R}\frac{\partial \Psi}{\partial X}; \tag{2.1}$$

$$\left[U\frac{\partial U}{\partial X} + V\frac{\partial U}{\partial R}\right] + \frac{\partial P}{\partial X} = \left[\frac{1}{R}\frac{\partial (RT)}{\partial R} + \frac{\partial M}{\partial X}\right], \tag{2.2a}$$

$$\left[U\frac{\partial V}{\partial X} + V\frac{\partial V}{\partial R}\right] + \frac{\partial P}{\partial R} = \left[\frac{1}{R}\frac{\partial (RN)}{\partial R} + \frac{\partial T}{\partial X}\right]. \tag{2.2b}$$

The farfield and centerline boundary conditions for (2.1) and (2.2) are

$$U, V, P, T, M, N \rightarrow 0 \text{ as } R \rightarrow \infty; \tag{2.3a}$$

$$V, \frac{\partial U}{\partial R}, T \rightarrow 0, \; U \rightarrow \text{finite as } R \rightarrow 0. \tag{2.3b}$$

The downstream analysis considered here does not address the initial conditions.

3. THE DOWNSTREAM CORE REGION

Attention is directed to the flow region far downstream of the nozzle exit, characterized by $x = \delta X$ and $r = R$, with $x, r \sim O(1)$, and with the stretching parameter $\delta << 1$, such that $(R/X) = \delta(r/x) \sim O(\delta)$. (In § 6, from a comparison of theory and experiment, it is determined that $\delta \sim O(10^{-1})$.) The flow quantities for this downstream region are, in turn, scaled as

$$\Psi(X, R; \ldots) = \psi(x, r; \delta): \quad U = u, \; V = \delta v, \tag{3.1a}$$

$$P(X, R; \ldots) = \delta p(x, r; \delta), \tag{3.1b}$$

$$T(X, R; \ldots) = \delta \tau(x, r; \delta),$$

$$M(X, R; \ldots) = \delta \mu(x, r; \delta), \quad N(X, R; \ldots) = \delta \nu(x, r; \delta). \tag{3.1c}$$

Thus, the differential equations of mean motion in this region are

$$\frac{\partial u}{\partial x} + \frac{1}{r}\frac{\partial (rv)}{\partial r} = 0: \quad u = \frac{1}{r}\frac{\partial \psi}{\partial r}, \; v = -\frac{1}{r}\frac{\partial \psi}{\partial x}; \tag{3.2}$$

$$\left[u\frac{\partial u}{\partial x} + v\frac{\partial u}{\partial r}\right] + \delta\frac{\partial p}{\partial x} = \left[\frac{1}{r}\frac{\partial (r\tau)}{\partial r} + \delta\frac{\partial \mu}{\partial x}\right], \tag{3.3a}$$

$$\delta\left[u\frac{\partial v}{\partial x} + v\frac{\partial v}{\partial r}\right] + \frac{\partial p}{\partial r} = \left[\frac{1}{r}\frac{\partial (r\nu)}{\partial r} + \delta\frac{\partial \tau}{\partial x}\right]. \tag{3.3b}$$

The centerline boundary conditions are, now,

$$v, \frac{\partial u}{\partial r}, \tau \to 0, \; u \to \text{finite as } r \to 0. \tag{3.4}$$

In turn, (3.2)-(3.4) can be combined to give the following integral relations:

$$\frac{\partial}{\partial x}\left[\int_0^r u\rho \, d\rho\right] = -rv, \tag{3.5a}$$

$$\frac{\partial}{\partial x}\left[\int_0^r [u^2 + \delta(p-\mu)]\rho \, d\rho\right] = -r[uv-\tau], \tag{3.5b}$$

$$\delta\frac{\partial}{\partial x}\left[\int_0^r [uv-\tau]\rho \, d\rho\right] = -r\left[\left[p - \frac{1}{r}\int_0^r p \, d\rho - \nu\right] + \delta v^2\right]. \tag{3.5c}$$

As $r \to \infty$, subject to verification of the farfield behavior, it is taken that (3.5b) becomes

$$\frac{d}{dx}\left[\int_0^{\infty}[u^2 + \delta(p-\mu)]r\,dr\right] = -\left[r[uv-\tau]\right]_{,\infty} = 0:$$

$$\int_0^{\infty}[u^2 + \delta(p-\mu)]r\,dr \equiv (1/2)Z, \text{ const.} \tag{3.6}$$

For the self-similar formulation of this region, the independent and dependent variables are

$$\xi = x,\ \eta = \left[\frac{r}{x}\right]; \tag{3.7}$$

$$\psi(x, r; \delta) = \xi\, F(\eta; \delta): \quad u = \xi^{-1}\left[\frac{F'}{\eta}\right],\ v = -\xi^{-1}\left[\frac{F}{\eta} - F'\right], \tag{3.8a}$$

$$p(x, r; \delta) = \xi^{-2}\,\Pi(\eta; \delta), \tag{3.8b}$$

$$\tau(x, r; \delta) = \xi^{-2}\,\Phi(\eta; \delta),$$

$$\mu(x, r; \delta) = \xi^{-2}\,J(\eta; \delta),\ \nu(x, r; \delta) = \xi^{-2}\,K(\eta; \delta). \tag{3.8c}$$

Introduction of (3.7) and (3.8) into (3.2) and (3.3) produces

$$\left[\left\{\eta\Phi + F\left[\frac{F'}{\eta}\right]\right\} + \delta\left\{\eta^2(\Pi-J)\right\}\right]' = 0, \tag{3.9a}$$

$$\left[\left\{\eta(\Pi-K)\right\} + \delta\left\{\eta^2\Phi + F\left[\frac{F}{\eta} - F'\right]\right\}\right]' = \Pi. \tag{3.9b}$$

The primes in (3.8) and (3.9) denote differentiation with respect to η. The centerline boundary conditions are

$$F,\ F',\ \Phi \to 0,\ \left[\frac{F'}{\eta}\right] \to \left[\frac{F'}{\eta}\right]_{,0} \text{ as } \eta \to 0. \tag{3.10}$$

In this self-similar formulation, (3.6) becomes

$$\int_0^{\infty}\left[\left[\frac{F'}{\eta}\right]^2 + \delta(\Pi-J)\right]\eta\,d\eta = (1/2)Z. \tag{3.11}$$

The introduction of the pressure-integral function, Λ, defined by

$$\Lambda = \int_0^\eta \Pi \, d\eta' \text{, such that } \Pi = \Lambda' \text{,} \tag{3.12}$$

leads to the following self-similar boundary-value problem for the downstream core region of the turbulent round jet:

$$\left[\left\{\eta\Phi + F\left[\frac{F'}{\eta}\right]\right\} + \delta\left\{\eta^2(\Lambda' - J)\right\}\right] = 0, \tag{3.13a}$$

$$\left[\left\{\eta(\Lambda' - K) - \Lambda\right\} + \delta\left\{\eta^2\Phi + F\left[\frac{F}{\eta} - F'\right]\right\}\right] = 0; \tag{3.13b}$$

$$F, F', \Lambda, \Phi \to 0, \left[\frac{F'}{\eta}\right] \to \left[\frac{F'}{\eta}\right]_o \text{ as } \eta \to 0; \tag{3.14}$$

$$\int_0^\infty \left[\left[\frac{F'}{\eta}\right]^2 + \delta(\Lambda' - J)\right]\eta \, d\eta = (1/2)Z. \tag{3.15}$$

A more detailed examination of this self-similar downstream region is facilitated with the introduction of the following asymptotic representations:

$$G(\eta; \delta) \cong G_o(\eta) + \delta G_1(\eta) + \ldots, \text{ with } G = F, \Lambda, \Phi, J, K. \tag{3.16}$$

Thus, the zeroth- and first-order boundary-value problems are

$$\left[\eta\Phi_o + F_o\left[\frac{F_o'}{\eta}\right]\right] = 0, \tag{3.17a}$$

$$\left[\eta(\Lambda_o' - K_o) - \Lambda_o\right] = 0: \quad \Pi_o = \Lambda_o', \; K_o = \eta\left[\frac{\Lambda_o}{\eta}\right]', \tag{3.17b}$$

$$F_o, F_o', \Lambda_o, \Phi_o \to 0, \left[\frac{F_o'}{\eta}\right] \to B_o \text{ as } \eta \to 0, \tag{3.17c}$$

$$\int_0^\infty \left[\frac{F_o'}{\eta}\right]^2 \eta \, d\eta = (1/2)Z; \tag{3.17d}$$

$$\left[\eta\Phi_1 + F_0\left(\frac{F_1'}{\eta}\right) + \left(\frac{F_0'}{\eta}\right)F_1\right] = -\left[\eta^2(\Lambda_0'-J_0)\right], \tag{3.18a}$$

$$\left[\eta(\Lambda_1'-K_1)-\Lambda_1\right] = -\left[\eta^2\Phi_0 + F_0\left(\frac{F_0}{\eta} - F_0'\right)\right] = \left[\eta\left(\frac{F_0^2}{\eta}\right)'\right]:$$

$$\Pi_1 = \Lambda_1', \; K_1 = \left[\eta\left(\frac{\Lambda_1}{\eta}\right)' - \left(\frac{F_0^2}{\eta}\right)'\right], \tag{3.18b}$$

$$F_1, \; F_1', \; \Lambda_1, \; \Phi_1 \to 0, \; \left(\frac{F_1'}{\eta}\right) \to B_1 \text{ as } \eta \to 0, \tag{3.18c}$$

$$\int_0^\infty \left(\frac{F_0'}{\eta}\right)\left(\frac{F_1'}{\eta}\right)\eta \, d\eta = -\frac{1}{2}\int_0^\infty (\Lambda_0'-J_0)\eta \, d\eta. \tag{3.18d}$$

To proceed, based on experiment and theory (as reported by Hinze 1975, Schlichting 1979, and others), the zeroth-order approximation for the axial-velocity function is taken to be

$$\left(\frac{F_0'}{\eta}\right) = \frac{B_0}{(1 + c^2\eta^2)^2} = B_0 \frac{1}{(1 + k)^2}, \tag{3.19a}$$

where $k = c^2\eta^2$. Introduction of (3.19a) into (3.17d) yields $(B_0/c) = (3Z)^{1/2}$. In what follows, it is taken that $B_0 = 1$, and, in turn, $c = (3Z)^{-1/2}$. The farfield and centerline behaviors for this function are

$$\left(\frac{F_0'}{\eta}\right) \to k^{-2}\left[1-2k^{-1} + \ldots\right] \to 0 \text{ as } k \to \infty, \tag{3.19b}$$

$$\left(\frac{F_0'}{\eta}\right) \to (1-2k + \ldots) \to 1 \text{ as } k \to 0. \tag{3.19c}$$

The corresponding approximation for the streamfunction is

$$F_0 = \frac{B_0 \, \eta^2}{2(1 + c^2\eta^2)} = A_0 \frac{k}{(1+k)}, \text{ with } A_0 = (3/2)Z: \tag{3.20a}$$

$$F_0 \to A_0 (1-k^{-1} + \ldots) \to A_0 \text{ as } k \to \infty, \tag{3.20b}$$

$$F_0 \to A_0 \, k(1-k + \ldots) \to 0 \text{ as } k \to 0. \tag{3.20c}$$

From (3.19) and (3.20), the zeroth-order radial-velocity function is

$$\left(\frac{F_o}{\eta} - F_o'\right) = - \frac{B_o \eta (1 - c^2\eta^2)}{2(1 + c^2\eta^2)^2} = - \frac{1}{2c} \frac{k^{1/2}(1-k)}{(1+k)^2}: \tag{3.21a}$$

$$\left(\frac{F_o}{\eta} - F_o'\right) \to \frac{1}{2c} k^{-1/2}(1-3k^{-1} + \ldots) \to 0 \text{ as } k \to \infty, \tag{3.21b}$$

$$\left(\frac{F_o}{\eta} - F_o'\right) \to - \frac{1}{2c} k^{1/2}(1-3k + \ldots) \to 0 \text{ as } k \to 0. \tag{3.21c}$$

The leading-order approximation for the shear-stress function, in turn, is

$$\Phi_o = - \frac{F_o}{\eta}\left(\frac{F_o'}{\eta}\right) = - \frac{B_o^2 \eta}{2(1 + c^2\eta^2)^3} = - \frac{1}{2c} \frac{k^{1/2}}{(1 + k)^3} : \tag{3.22a}$$

$$\Phi_o \to - \frac{1}{2c} k^{-5/2}(1-3k^{-1} + \ldots) \to 0 \text{ as } k \to \infty, \tag{3.22b}$$

$$\Phi_o \to - \frac{1}{2c} k^{1/2} (1- 3k + \ldots) \to 0 \text{ as } k \to 0. \tag{3.22c}$$

The experimental work of Wygnanski & Fiedler (1969) suggests the following approximations for J_o and K_o:

$$J_o = - \frac{a_o}{(1 + c^2\eta^2)^2} = -a_o \frac{1}{(1 + k)^2}, \text{ with } 0 < a_o < 1: \tag{3.23a}$$

$$J_o \to -a_o k^{-2}(1-2k^{-1} + \ldots) \to 0 \text{ as } k \to \infty, \tag{3.23b}$$

$$J_o \to -a_o(1-2k + \ldots) \to -a_o \text{ as } k \to 0; \tag{3.23c}$$

$$K_o = - \frac{b_o}{(1 + c^2\eta^2)^2} = -b_o \frac{1}{(1 + k)^2}, \text{ with } 0 < b_o < a_o < 1: \tag{3.24a}$$

$$K_o \to -b_o k^{-2}(1-2k^{-1} + \ldots) \to 0 \text{ as } k \to \infty, \tag{3.24b}$$

$$K_o \to -b_o(1-2k + \ldots) \to -b_o \text{ as } k \to 0. \tag{3.24c}$$

The evaluation of a_o and b_o from experimental data is presented in § 6.

From (3.17b), it follows that

$$\Lambda_o = \frac{b_o}{2c}\, k^{1/2}\left[\ell n\left\{\frac{(1+k)}{k}\right\} - \frac{1}{(1+k)}\right]: \tag{3.25a}$$

$$\Lambda_o \to \frac{b_o}{4c}\, k^{-3/2}(1 - \frac{4}{3}\, k^{-1} + \ldots) \to 0 \text{ as } k \to \infty, \tag{3.25b}$$

$$\Lambda_o \to \frac{b_o}{2c}\, k^{1/2}\left[\ell n(k^{-1}) - 1 + 2k - + \ldots\right] \to 0 \text{ as } k \to 0. \tag{3.25c}$$

Thus, the leading-order approximation for the pressure function is

$$\Pi_o = \Lambda_o' = \frac{b_o}{2}\left[\ell n\left\{\frac{(1+k)}{k}\right\} - \frac{(3+k)}{(1+k)^2}\right]: \tag{3.26a}$$

$$\Pi_o \to -\frac{3b_o}{4}\, k^{-2}\left[1 - \frac{20}{9}\, k^{-1} + \ldots\right] \to 0 \text{ as } k \to \infty, \tag{3.26b}$$

$$\Pi_o \to \frac{b_o}{2}\left[\ell n(k^{-1}) - 3 + 6k + \ldots\right] \to \infty \text{ as } k \to 0. \tag{3.26c}$$

The logarithmic blow-up of the "models" for Λ_o and Π_o as $k \to 0$ is noted. No further consideration is given to the centerline blow-up, as the emphasis of this paper is on the effect of the "models" for the pressure and normal stresses on the farfield behavior.

Now, the first-order approximation for the axial-velocity function is taken to be

$$\left(\frac{F_1'}{\eta}\right) = B_1\, \frac{1}{(1+k)^2}, \text{ with } B_1 = -(3/4)(2a_o - b_o) < 0: \tag{3.27a}$$

$$\left(\frac{F_1'}{\eta}\right) \to B_1 k^{-2}(1 - 2k^{-1} + \ldots) \to 0 \text{ as } k \to \infty, \tag{3.27b}$$

$$\left(\frac{F_1'}{\eta}\right) \to B_1(1 - 2k + \ldots) \to B_1 \text{ as } k \to 0. \tag{3.27c}$$

The value of B_1 is determined from the first-order momentum integral relation, (3.18d), with $B_0 = 1$. The corresponding streamfunction is

$$F_1 = A_1 \frac{k}{(1+k)}, \text{ with } A_1 = -(9/8)(2a_0 - b_0)Z < 0: \tag{3.28a}$$

$$F_1 \to A_1(1 - k^{-1} + \ldots) \to A_1 \text{ as } k \to \infty, \tag{3.28b}$$

$$F_1 \to A_1 k(1 - k + \ldots) \to 0 \text{ as } k \to 0. \tag{3.28c}$$

The first-order radial-velocity function is

$$\left[\frac{F_1}{\eta} - F_1'\right] = \frac{B_1}{2c} \frac{k^{1/2}(1-k)}{(1+k)^2}: \tag{3.29a}$$

$$\left[\frac{F_1}{\eta} - F_1'\right] \to \frac{B_1}{2c} k^{-1/2}(1 - 3k^{-1} + \ldots) \to 0 \text{ as } k \to \infty, \tag{3.29b}$$

$$\left[\frac{F_1}{\eta} - F_1'\right] \to -\frac{B_1}{2c} k^{1/2}(1 - 3k + \ldots) \to 0 \text{ as } k \to 0. \tag{3.29c}$$

The resulting first-order approximation for the shear-stress function is

$$\Phi_1 = -\left[\frac{F_0}{\eta}\left(\frac{F_1'}{\eta}\right) + \left(\frac{F_0'}{\eta}\right)\frac{F_1}{\eta} + \eta(\Pi_0 - J_0)\right]$$

$$= -\frac{k^{1/2}}{c}\left\{\frac{b_0}{2}\left[\ell n\left\{\frac{(1+k)}{k}\right\} - \frac{1}{(1+k)}\right] + \frac{(a_0 - b_0)}{(1+k)^2} - \frac{(3/4)(2a_0 - b_0)}{(1+k)^3}\right\}: \tag{3.30a}$$

$$\Phi_1 \to -\frac{k^{-3/2}}{4c}\left[(4a_0 - 3b_0) - \frac{1}{3}(42a_0 - 29b_0)k^{-1} + \ldots\right] \to 0 \text{ as } k \to \infty, \tag{3.30b}$$

$$\Phi_1 \to -\frac{k^{1/2}}{2c}\left[b_0 \ell n(k^{-1}) - \frac{1}{2}(2a_0 + 3b_0) + \frac{1}{2}(10a_0 + 3b_0)k + \ldots\right] \to 0 \text{ as } k \to 0. \tag{3.30c}$$

Here, the approximations for J_1 and K_1 are taken to be

$$J_1 = -a_1 \frac{1}{(1+k)^2}, \text{ with } a_1 = \text{const. (to be specified):} \tag{3.31a}$$

$$J_1 \to -a_1 k^{-2}(1-2k^{-1} + \ldots) \to 0 \text{ as } k \to \infty, \tag{3.31b}$$

$$J_1 \to -a_1 (1-2k + \ldots) \to -a_1 \text{ as } k \to 0; \tag{3.31c}$$

$$K_1 = -b_1 \frac{1}{(1+k)^2}, \text{ with } b_1 = \text{const. (to be specified):} \tag{3.32a}$$

$$K_1 \to -b_1 k^{-2}(1-2k^{-1} + \ldots) \to 0 \text{ as } k \to \infty, \tag{3.32b}$$

$$K_1 \to -b_1 (1-2k + \ldots) \to -b_1 \text{ as } k \to 0. \tag{3.32c}$$

From (3.18b), it is determined that, subject to the pertinent boundary conditions,

$$\Lambda_1 = -\frac{A_0}{4c} \frac{k^{1/2}(1-k)}{(1+k)^2} + \frac{b_1}{2c}\left[\ell n\left\{\frac{(1+k)}{k}\right\} - \frac{1}{(1+k)}\right]. \tag{3.33}$$

In turn,

$$\Pi_1 = \Lambda_1' = -\frac{A_0}{4} \frac{(1-6k+k^2)}{(1+k)^3} + \frac{b_1}{2}\left[\ell n\left\{\frac{(1+k)}{k}\right\} - \frac{(3+k)}{(1+k)^2}\right]: \tag{3.34a}$$

$$\Pi_1 \to -\frac{A_0}{4}k^{-1}(1 -9k^{-1} + \ldots) - \frac{3b_1}{4}k^{-2}(1 - + \ldots) \to 0 \text{ as } k \to \infty, \tag{3.34b}$$

$$\Pi_1 \to -\frac{A_0}{4}(1 -9k + \ldots) + \frac{b_1}{2}[\ell n(k^{-1}) -3 + 6k + \ldots] \to \infty \text{ as } k \to 0. \tag{3.34c}$$

Higher-order solutions for the core-region flow quantities are not considered here. It is noted, nevertheless, that a preliminary study of the second-order boundary-value problems indicates that the farfield behavior of the velocity solutions of this order is such that the momentum-integral relation of (3.11) fails. This failure stems from the interaction of the core-region quantities with those of the intermediate region, analyzed in § 4.

From the preceding developments, it is now possible to determine the farfield behavior of the solutions in the limit of $\eta \to \infty$, $\delta \to 0$, such that $\theta = \delta^{1/2}\eta \sim O(1)$. In this limit, $k = c^2\eta^2 = (1/3Z)\delta^{-1}\theta^2 \to \infty$; and

$$F \cong F_0 + \delta F_1 + \ldots$$

$$\to \left[(3/2)Z - \delta\left\{(9/2)Z^2\theta^{-2} + (9/8)(2a_0 - b_0)Z + \ldots\right\} + O(\delta^2)\right], \qquad (3.35a)$$

$$\left(\frac{F'}{\eta}\right) \cong \left(\frac{F'_0}{\eta}\right) + \delta\left(\frac{F'_1}{\eta}\right) + \ldots$$

$$\to \delta^2\left[\left\{9Z^2\theta^{-4} + \ldots\right\} + O(\delta)\right], \qquad (3.35b)$$

$$\left(\frac{F}{\eta} - F'\right) \cong \left(\frac{F_0}{\eta} - F'_0\right) + \delta\left(\frac{F_1}{\eta} - F'_1\right) + \ldots$$

$$\to \delta^{1/2}\left[(3/2)Z\theta^{-1} - \delta\left\{(27/2)Z^2\theta^{-3} + (9/8)(2a_0 - b_0)Z\theta^{-1} + \ldots\right\} + O(\delta^2)\right]; \qquad (3.35c)$$

$$\Phi \cong \Phi_0 + \delta\Phi_1 + \ldots$$

$$\to -\delta^{5/2}\left[\left\{(27/2)Z^3\theta^{-5} + (9/4)(4a_0 - 3b_0)Z^2\theta^{-3} + \ldots\right\} + O(\delta)\right], \qquad (3.36a)$$

$$J \cong J_0 + \delta J_1 + \ldots$$

$$\to -\delta^2\left[\left\{9a_0Z^2\theta^{-4} + \ldots\right\} + O(\delta)\right], \qquad (3.36b)$$

$$K \cong K_0 + \delta K_1 + \ldots$$

$$\to -\delta^2\left[\left\{9b_0Z^2\theta^{-4} + \ldots\right\} + O(\delta)\right]; \qquad (3.36c)$$

$$\Pi \cong \Pi_0 + \delta\Pi_1 + \ldots$$

$$\to -\delta^2\left[\left\{(27/4)b_0Z^2\theta^{-4} + (9/8)Z^2\theta^{-2} + \ldots\right\} + O(\delta)\right]. \qquad (3.37)$$

4. THE DOWNSTREAM INTERMEDIATE REGION

The results of (3.35)-(3.37) indicate that, to ensure uniform validity, a region exterior to the downstream core region is required. For this region, designated, here, as the downstream intermediate region, the appropriate scalings of the original independent and dependent variables are

$$x_k = \delta X, \; r_k = \delta^{1/2} R; \tag{4.1}$$

$$\Psi(X, R; \delta) = A_0 x_k + \delta \psi_k(x_k, r_k; \delta): \; U = \delta^2 u_k, \; V = -\delta^{3/2}\frac{A_0}{r_k} + \delta^{5/2} v_k, \tag{4.2a}$$

$$P(X, R; \delta) = \delta^3 p_k(x_k, r_k; \delta), \tag{4.2b}$$

$$T(X, R; \delta) = \delta^{7/2} \tau_k(x_k, r_k; \delta),$$

$$M(X, R; \delta) = \delta^3 \mu_k(x_k, r_k; \delta), \; N(X, R; \delta) = \delta^3 \nu_k(x_k, r_k; \delta). \tag{4.2c}$$

These variables are related to those of the core region through

$$x_k = x, \; r_k = \delta^{1/2} r;$$

$$\psi = A_0 x_k + \delta \psi_k, \text{ with } A_0 = (3/2)Z: \quad u = \delta^2 u_k, \; v = \delta^{1/2}\left[-\frac{A_0}{r_k} + \delta v_k\right],$$

$$p = \delta^2 p_k, \; \tau = \delta^{5/2}\tau_k, \; \mu = \delta^2 \mu_k, \; \nu = \delta^2 \nu_k. \tag{4.3}$$

Introduction of (4.1) and (4.2) into (2.1) and (2.2) produces

$$\frac{\partial u_k}{\partial x_k} + \frac{1}{r_k}\frac{\partial (r_k v_k)}{\partial r_k} = 0: \quad u_k = \frac{1}{r_k}\frac{\partial \psi_k}{\partial r_k}, \; v_k = -\frac{1}{r_k}\frac{\partial \psi_k}{\partial x_k}; \tag{4.4}$$

$$-\frac{A_0}{r_k}\frac{\partial u_k}{\partial r_k} + \delta\left[u_k \frac{\partial u_k}{\partial x_k} + v_k \frac{\partial u_k}{\partial r_k}\right] + \frac{\partial p_k}{\partial x_k} = \left[\frac{1}{r_k}\frac{\partial (r_k \tau_k)}{\partial r_k} + \frac{\partial \mu_k}{\partial x_k}\right], \tag{4.5a}$$

$$-\frac{A_0^2}{r_k^3} - \delta A_0 \frac{\partial}{\partial r_k}\left(\frac{v_k}{r_k}\right) + \delta^2\left[u_k \frac{\partial v_k}{\partial x_k} + v_k \frac{\partial v_k}{\partial r_k}\right] + \frac{\partial p_k}{\partial r_k} = \left[\frac{1}{r_k}\frac{\partial (r_k \nu_k)}{\partial r_k} + \delta\frac{\partial \tau_k}{\partial x_k}\right]. \tag{4.5b}$$

A self-similar formulation of this intermediate region is sought through the introduction of the following variables:

$$\xi = x_k, \quad \theta = (r_k/x_k); \tag{4.6}$$

$$\psi_k(x_k, r_k; \delta) = \xi F_k(\theta; \delta): \quad u_k = \xi^{-1}\left[\frac{F_k'}{\theta}\right], \quad v_k = -\xi^{-1}\left[\frac{F_k}{\theta} - F_k'\right], \tag{4.7a}$$

$$p_k(x_k, r_k; \delta) = \xi^{-2}\Pi_k(\theta; \delta) \equiv \xi^{-2}\Lambda_k'(\theta; \delta), \tag{4.7b}$$

$$\tau_k(x_k, r_k; \delta) = \xi^{-2}\Phi_k(\theta; \delta),$$

$$\mu_k(x_k, r_k; \delta) = \xi^{-2}J_k(\theta; \delta), \quad \nu_k(x_k, r_k; \delta) = \xi^{-2}K_k(\theta; \delta). \tag{4.7c}$$

The independent variables of the intermediate region are related to those of the core region by

$$\xi = x_k = x, \quad \theta = (r_k/x_k) = \delta^{1/2}(r/x) = \delta^{1/2}\eta. \tag{4.8}$$

The resulting self-similar axial- and radial-momentum equations are

$$\left[\left\{\theta\left[\Phi_k + \frac{A_0}{\theta}\left[\frac{F_k'}{\theta}\right]\right] + \theta^2\left[\Lambda_k' - J_k\right]\right\} + \delta\left\{F_k\left[\frac{F_k'}{\theta}\right]\right\}\right] = 0, \tag{4.9a}$$

$$\left[\left\{\theta\left[\left[\Lambda_k' - \frac{\Lambda_k}{\theta} - K_k\right] + \frac{A_0^2}{\theta^2}\right]\right\} + \delta\left\{\theta^2\Phi_k + A_0\left[2\frac{F_k}{\theta} - F_k'\right]\right\} + \delta^2\left\{F_k\left[\frac{F_k}{\theta} - F_k'\right]\right\}\right] = 0. \tag{4.9b}$$

Again, it is appropriate to introduce asymptotic representations for the dependent variables, i.e.,

$$G_k(\theta;\delta) \cong G_{k0}(\theta) + \ldots, \quad \text{with } G_k = F_k, \Lambda_k, \Phi_k, J_k, K_k. \tag{4.10}$$

Thus, the zeroth-order equations for the intermediate region are

$$\left[\Phi_{k0} + \frac{A_0}{\theta}\left[\frac{F_{k0}'}{\theta}\right] + \theta\left[\Lambda_{k0}' - J_{k0}\right]\right] = 0, \tag{4.11a}$$

$$\left[\left[\Lambda_{k0}' - \frac{\Lambda_{k0}}{\theta} - K_{k0}\right] + \frac{A_0^2}{\theta^2}\right] = 0. \tag{4.11b}$$

The solutions of (4.11) that match to those of the (farfield) core region are

$$F_{k0} = \left\{\frac{1}{4}A_0\theta^2 + A_1 - 2A_0^2\theta^{-2}\right\}: \tag{4.12a}$$

$$\left[\frac{F'_{k0}}{\theta}\right] = \left\{\frac{1}{2}A_0 + 4A_0^2\theta^{-4}\right\}, \left[\frac{F_{k0}}{\theta} - F'_{k0}\right] = -\left\{\frac{1}{4}A_0\theta - A_1\theta^{-1} + 6A_0^2\theta^{-3}\right\}; \tag{4.12b,c}$$

$$\Phi_{k0} = -\left\{\frac{1}{2}A_0\theta^{-1} + \left[4a_0 - 3b_0\right]A_0^2\theta^{-3} + 4A_0^3\theta^{-5}\right\}, \tag{4.13a}$$

$$J_{k0} = -\left\{\mu_0\theta^{-2} + 4a_0A_0^2\theta^{-4}\right\}, K_{k0} = -\left\{\nu_0\theta^{-2} + 4b_0A_0^2\theta^{-4}\right\}, \text{ with } (2\mu_0 - \nu_0) = A_0^2; \tag{4.13b,c}$$

$$\Pi_{k0} = -\left\{\mu_0\theta^{-2} + 3b_0A_0^2\theta^{-4}\right\}. \tag{4.14}$$

Recall that $A_0 = (3/2)Z$, $A_1 = -(9/8)(2a_0 - b_0)Z$, ... Higher-order solutions for this intermediate region are not pursued here.

In the limit of $\theta \to \infty$, $\delta \to 0$, such that $\zeta = \delta^{1/2}\theta \sim O(1)$, the variables of the intermediate region have the following behaviors:

$$F_k \cong F_{k0} + \ldots \to \delta^{-1}\left[(1/4)A_0\zeta^2 + O(\delta)\right], \tag{4.15a}$$

$$\left[\frac{F'_k}{\theta}\right] \cong \left[\frac{F'_{k0}}{\theta}\right] + \ldots \to \left[(1/2)A_0 + O(\delta)\right], \tag{4.15b}$$

$$\left[\frac{F_k}{\theta} - F'_k\right] \cong \left[\frac{F_{k0}}{\theta} - F'_{k0}\right] + \ldots \to -\delta^{-1/2}\left[(1/4)A_0\zeta + O(\delta)\right]; \tag{4.15c}$$

$$\Phi_k \cong \Phi_{k0} + \ldots \to -\delta^{1/2}\left[(1/2)A_0^2\zeta^{-1} + O(\delta)\right], \tag{4.16a}$$

$$J_k \cong J_{k0} + \ldots \to -\delta\left[\mu_0\zeta^{-2} + O(\delta)\right], \tag{4.16b}$$

$$K_k \cong K_{k0} + \ldots \to -\delta\left[\nu_0\zeta^{-2} + O(\delta)\right]; \tag{4.16c}$$

$$\Pi_k \cong \Pi_{k0} + \ldots \to -\delta\left[\mu_0\zeta^{-2} + O(\delta)\right]. \tag{4.17}$$

5. THE DOWNSTREAM EXTERIOR REGION

The uniformly valid characterization of the farfield development of the turbulent round jet is completed through the introduction of the downstream exterior region, wherein the appropriate variables are

$$x_s = \delta X, \; r_s = \delta R; \tag{5.1}$$

$$\Psi(X, R; \delta) = \psi_s(x_s, r_s; \delta): \quad U = \delta^2 u_s, \; V = \delta^2 v_s, \tag{5.2a}$$

$$P(X, R; \delta) = \delta^4 p_s(x_s, r_s; \delta), \tag{5.2b}$$

$$T(X, R; \delta) = \delta^4 \tau_s(x_s, r_s; \delta),$$

$$M(X, R; \delta) = \delta^4 \mu_s(x_s, r_s; \delta), \; N(X, R; \delta) = \delta^4 \nu_s(x_s, r_s; \delta). \tag{5.2c}$$

In this region, the vorticity is

$$\Omega(X, R; \delta) = \left[\frac{\partial V}{\partial X} - \frac{\partial U}{\partial R}\right] = \delta^3 \omega_s(x_s, r_s; \delta) = \delta^3 \left[\frac{\partial v_s}{\partial x_s} - \frac{\partial u_s}{\partial r_s}\right]. \tag{5.3}$$

In terms of these exterior-region variables, the equations of motion are

$$\frac{\partial u_s}{\partial x_s} + \frac{1}{r_s}\frac{\partial (r_s v_s)}{\partial r_s} = 0: \quad u_s = \frac{1}{r_s}\frac{\partial \psi_s}{\partial r_s}, \; v_s = -\frac{1}{r_s}\frac{\partial \psi_s}{\partial x_s}; \tag{5.4}$$

$$\left[u_s \frac{\partial u_s}{\partial x_s} + v_s \frac{\partial u_s}{\partial r_s}\right] + \frac{\partial p_s}{\partial x_s} = \left[\frac{1}{r_s}\frac{\partial (r_s \tau_s)}{\partial r_s} + \frac{\partial \mu_s}{\partial x_s}\right], \tag{5.5a}$$

$$\left[u_s \frac{\partial v_s}{\partial x_s} + v_s \frac{\partial v_s}{\partial r_s}\right] + \frac{\partial p_s}{\partial r_s} = \left[\frac{1}{r_s}\frac{\partial (r_s \nu_s)}{\partial r_s} + \frac{\partial \tau_s}{\partial x_s}\right]. \tag{5.5b}$$

Taking this exterior region to be an irrotational one, (5.3) becomes

$$\left[\frac{\partial v_s}{\partial x_s} - \frac{\partial u_s}{\partial r_s}\right] = -\left[\frac{\partial^2 \psi_s}{\partial x_s^2} + r_s \frac{\partial}{\partial r_s}\left[\frac{1}{r_s}\frac{\partial \psi_s}{\partial r_s}\right]\right] = 0. \tag{5.6}$$

The boundary conditions for these equations are

$$u_s,\ v_s,\ p_s,\ \tau_s,\ \mu_s,\ \nu_s \to 0 \text{ as } r_s \to \infty. \tag{5.7}$$

Again, a self-similar formulation is sought for this region in terms of the following variables:

$$\xi = x_s,\ \zeta = (r_s/x_s); \tag{5.8}$$

$$\psi_s(x_s, r_s; \delta) = \xi F_s(\zeta; \delta):$$

$$u_s = \xi^{-1}\left(\frac{F_s'}{\zeta}\right),\ v_s = -\xi^{-1}\left(\frac{F_s}{\zeta} - F_s'\right),$$

$$\omega_s = -\xi^{-2}\left[\frac{(1+\zeta^2)}{\zeta}\left\{F_s' - \frac{\zeta}{(1+\zeta^2)}F_s\right\}\right]', \tag{5.9a}$$

$$p_s(x_s, r_s; \delta) = \xi^{-2}\Pi_s(\zeta; \delta) \equiv \xi^{-2}\Lambda_s'(\zeta; \delta), \tag{5.9b}$$

$$\tau_s(x_s, r_s; \delta) = \xi^{-2}\Phi_s(\zeta; \delta),$$

$$\mu_s(x_s, r_s; \delta) = \xi^{-2}J_s(\zeta; \delta).\ \nu_s(x_s, r_s; \delta) = \xi^{-2}K_s(\zeta; \delta). \tag{5.9c}$$

Note that $\zeta = (r_s/x_s) = (R/X) = \delta^{1/2}\theta = \delta\eta$.

In turn, (5.5) and (5.6), subject to (5.7), can be written as

$$\left[\left\{\Phi_s + \left(\frac{F_s'}{\zeta}\right)\left(\frac{F_s}{\zeta} - F_s'\right)\right\} + \zeta\left\{\left(\Lambda_s' - J_s\right) + \left(\frac{F_s'}{\zeta}\right)^2\right\}\right] = 0, \tag{5.10a}$$

$$\left[\left\{\left(\Lambda_s' - \frac{\Lambda_s}{\zeta} - K_s\right) + \left(\frac{F_s}{\zeta} - F_s'\right)^2\right\} + \zeta\left\{\Phi_s + \left(\frac{F_s'}{\zeta}\right)\left(\frac{F_s}{\zeta} - F_s'\right)\right\}\right] = 0; \tag{5.10b}$$

$$\left[\frac{(1+\zeta^2)}{\zeta}\left\{F_s' - \frac{\zeta}{(1+\zeta^2)}F_s\right\}\right]' = 0. \tag{5.11}$$

An asymptotic analysis of this region, in terms of expansion of the form

$$G_s(\zeta;\delta) \cong G_{s0}(\zeta) + \ldots, \quad \text{with } G_s = F_s,\ \Lambda_s,\ \Phi_s,\ J_s,\ K_s, \tag{5.12}$$

from a consideration of (5.10) and (5.11), leads to

$$F_{s0} = \frac{1}{2} A_0 \left[(1+\zeta^2)^{1/2} + 1\right]: \tag{5.13a}$$

$$\left[\frac{F'_{s0}}{\zeta}\right] = \frac{1}{2}A_0 \left[1+\zeta^2\right]^{-1/2}, \quad \left[\frac{F_{s0}}{\zeta} - F'_{s0}\right] = \frac{1}{2}A_0 \zeta^{-1}\left[1 + \left[1+\zeta^2\right]^{-1/2}\right]; \tag{5.13b,c}$$

$$\Phi_{s0} = -\left[\frac{F'_{s0}}{\zeta}\right]\left[\frac{F_{s0}}{\zeta} - F'_{s0}\right] = -\frac{1}{4}A_0^2\zeta^{-1}\left[1+\zeta^2\right]^{-1/2}\left[1 + \left[1+\zeta^2\right]^{-1/2}\right], \tag{5.14a}$$

$$\left[\Lambda'_{s0} - J_{s0}\right] = -\left[\frac{F'_{s0}}{\zeta}\right]^2 = -\frac{1}{4}A_0^2\left[1+\zeta^2\right]^{-1}, \tag{5.14b}$$

$$\left[\Lambda'_{s0} - \frac{\Lambda_{s0}}{\zeta} - K_{s0}\right] = -\left[\frac{F_{s0}}{\zeta} - F'_{s0}\right]^2 = -\frac{1}{4}A_0^2\zeta^{-2}\left[1 + \left[1+\zeta^2\right]^{-1/2}\right]^2. \tag{5.14c}$$

The results for the *velocity functions* of (5.13) are consistent with those reported by Landau & Lifshitz (1959). The results of (5.14) represent new information concerning the behavior of the stress functions in the farfield. Higher-order solutions for the exterior region are not pursued here.

The farfield ($\zeta \to \infty$) behaviors of these zeroth-order functions are

$$F_{s0} \sim \frac{1}{2} A_0 \zeta \left[1 + \zeta^{-1} + \ldots\right] \to \infty: \tag{5.15a}$$

$$\left[\frac{F'_{s0}}{\zeta}\right] \sim \frac{1}{2} A_0 \zeta^{-1}\left[1 - \frac{1}{2}\zeta^{-2} + \ldots\right] \to 0, \tag{5.15b}$$

$$\left[\frac{F_{s0}}{\zeta} - F'_{s0}\right] \sim \frac{1}{2} A_0 \zeta^{-1}\left[1 + \zeta^{-1} + \ldots\right] \to 0, \tag{5.15c}$$

$$\Phi_{s0} \sim -\frac{1}{4} A_0^2 \zeta^{-2}\left[1 + \ldots\right] \to 0, \tag{5.16a}$$

$$\left[\Lambda'_{s0} - J_{s0}\right] \sim -\frac{1}{4} A_0^2 \zeta^{-2}\left[1 + \ldots\right] \to 0, \tag{5.16b}$$

$$\left[\Lambda'_{s0} - \frac{\Lambda_{s0}}{\zeta} - K_{s0}\right] \sim -\frac{1}{4} A_0^2 \zeta^{-2}\left[1 + \ldots\right] \to 0. \tag{5.16c}$$

It is noted that the behaviors of the pressure and normal-stress functions are

$$\Pi_{s0} = \Lambda'_{s0} \sim -\pi_0 \zeta^{-2}(1 + \ldots),\ J_{s0} \sim -\alpha_0 \zeta^{-2}(1 + \ldots),\ K_{s0} \sim -\beta_0 \zeta^{-2}(1 + \ldots),$$

$$\text{if } (\pi_0 - \alpha_0),\ (2\pi_0 - \beta_0) = \frac{1}{4} A_0^2, \text{ i.e., } (\pi_0 + \alpha_0 - \beta_0) = 0. \tag{5.17}$$

The nearfield ($\zeta \to 0$) behaviors of these functions are

$$F_{s0} \sim A_0 \left[1 + \frac{1}{4} \zeta^2 + \ldots\right] \to A_0 : \tag{5.18a}$$

$$\left[\frac{F'_{s0}}{\zeta}\right] \sim \frac{1}{2} A_0 \left[1 - \frac{1}{2} \zeta^2 + \ldots\right] \to \frac{1}{2} A_0, \tag{5.18b}$$

$$\left[\frac{F_{s0}}{\zeta} - F'_{s0}\right] \sim A_0 \zeta^{-1} \left[1 - \frac{1}{4} \zeta^2 + \ldots\right] \to \infty; \tag{5.18c}$$

$$\Phi_{s0} \sim -\frac{1}{2} A_0^2 \zeta^{-1} \left[1 - \frac{3}{4} \zeta^2 + \ldots\right] \to -\infty, \tag{5.19a}$$

$$\left[\Lambda'_{s0} - J_{s0}\right] \sim -\frac{1}{4} A_0^2 \left[1 - \zeta^2 + \ldots\right] \to -\frac{1}{4} A_0^2, \tag{5.19b}$$

$$\left[\Lambda'_{s0} - \frac{\Lambda_{s0}}{\zeta} - K_{s0}\right] \sim -A_0^2 \zeta^{-2} \left[1 - \frac{1}{2} \zeta^2 + \ldots\right] \to -\infty. \tag{5.19c}$$

The behaviors of the pressure and normal-stress functions are

$$\Pi_{s0} = \Lambda'_{s0} \sim -\pi_0 \zeta^{-2}(1 + \ldots),\ J_{s0} \sim -\mu_0 \zeta^{-2}(1 + \ldots),\ K_{s0} \sim -\nu_0 \zeta^{-2}(1 + \ldots),$$

$$\text{if } \pi_0 = \mu_0 \text{ and } (2\mu_0 - \nu_0) = A_0^2. \tag{5.20}$$

It is seen that these functions (i) satisfy the boundary conditions at infinity, and (ii) match to the farfield behaviors of the intermediate-region functions.

6. RESULTS AND DISCUSSION

The experimental data for the centerline velocity as a function of axial distance are expressed, in the present notation, as

$$U_{\ell} = \frac{\tilde{U}_{\ell}}{\tilde{U}_j} \approx \frac{C}{\left[(\tilde{X}-\tilde{X}_o)/(2\tilde{B}_j)\right]} = \frac{2C}{X}, \text{ with } C = \text{const. (determined experimentally)}, \tag{6.1}$$

i.e., the centerline velocity is inversely proportional to the axial distance in the self-similar downstream zone. Hinze & Van der Hegge Zijnen (1949), hereinafter denoted as H-VdHZ, found $C \approx 5.9$, $(2C)^{-1} \approx 0.085$ for $20 < X < 100$; Wygnanski & Fiedler (1969), denoted as W-F, found $C \approx 5.4$, $(2C)^{-1} \approx 0.093$ for $50 < X < 180$. In the self-similar analysis of § 3, it is found that the centerline velocity is

$$U_{\ell} \cong \xi^{-1}[B_o + \delta B_1 + \ldots],$$

$$\text{with } \xi = \delta X,\ B_o = 1,\ B_1 = -(3/4)(2a_o - b_o),\ \ldots . \tag{6.2}$$

From the W-F data, $(\delta B_1) \approx -0.079$ (as is shown later in this section). A comparison of (6.1) and (6.2) indicates that, if terms of $O(\delta^2)$ are neglected,

$$(2C) \approx \delta^{-1}[1 + (\delta B_1)] \text{ and/or } \delta \approx (2C)^{-1}[1 + (\delta B_1)]:$$

$$\delta \approx 0.086 \text{ for } (2C)^{-1} \approx 0.093,\ (\delta B_1) \approx -0.079. \tag{6.3}$$

For the purpose of consistency only, hereafter, W-F is employed as the basis for comparison.

The axial-velocity-distribution data are (most often) presented as

$$U^* = \frac{U}{U_{\ell}} \approx \frac{1}{(1 + L^2\zeta^2)^2} \equiv U^*_{CORE}(\zeta; L),$$

$$\text{with } \zeta = (R/X),\ L^2 = \text{const.(determined experimentally)}. \tag{6.4}$$

The measurements of H-VdHZ give $L^2 \approx 63.8$; W-F find $L^2 \approx 57.8$. When terms of

$O(\delta^2)$ are neglected, the core-region analysis of § 3 shows that

$$U^* = \frac{U}{U_\ell} \approx \frac{1}{(1 + c^2\eta^2)^2}, \text{ with } \eta = \delta^{-1}(R/X),\ c = (3Z)^{-1/2}. \tag{6.5}$$

A comparison of (6.4) and (6.5) yields

$$L^2 \approx (3Z\delta^2)^{-1} \text{ and/or } Z \approx (3\delta^2 L^2)^{-1}:$$

$$Z \approx 0.78,\ c = (3Z)^{-1/2} \approx 0.65,\ A_0 = (3/2)Z \approx 1.2$$
$$\text{for } \delta \approx 0.086,\ L^2 \approx 57.8. \tag{6.6}$$

The farfield axial-velocity distribution determined by the zeroth-order exterior-region analysis of § 5, with $(1/2)\delta^2 A_0 = (4L^2)^{-1}$, is

$$U^* = \frac{U}{U_\ell} \approx \frac{(4L^2)^{-1}}{(1 + \zeta^2)^{1/2}} \equiv U^*_{EXT}(\zeta; L),$$
$$\text{with } (4L^2)^{-1} \approx 0.00433 \text{ for } L^2 \approx 57.8. \tag{6.7}$$

In figure 2a, $U^*_{CORE}(\zeta; L)$, given, by (6.4), is compared with the data of W-F. Not surprisingly, this representation compares well with the data. Figure 2b shows $U^*_{CORE}(\zeta; L)$ and $U^*_{EXT}(\zeta; L)$ of (6.4) and (6.7), respectively, as well as $U^*_{INTER}(\zeta; L)$, the intermediate-region representation. Since the data of W-F (and others) do not extend to the exterior region, as defined in this paper, it is not possible to make a farfield comparison.

When terms of $O(\delta^2)$ are neglected, the core-region radial-velocity distribution can be expressed as

$$V^* = \frac{V}{U_\ell} \approx \frac{\zeta(1-L^2\zeta^2)}{2(1 + L^2\zeta^2)^2} \equiv V^*_{CORE}(\zeta; L). \tag{6.8}$$

The zeroth-order exterior-region radial-velocity distribution is given by

$$V^* = \frac{V}{U_\ell} \approx -\frac{(4L^2)^{-1}[(1+\zeta^2)^{1/2} + 1]}{\zeta(1+\zeta^2)^{1/2}} \equiv V^*_{EXT}(\zeta; L). \tag{6.9}$$

Figure 3a compares $V^*_{CORE}(\zeta; L)$, of (6.8), with the data of W-F. Again, the comparison is good. The solutions $V^*_{CORE}(\zeta; L)$, $V^*_{EXT}(\zeta; L)$, and $V^*_{INTER}(\zeta; L)$

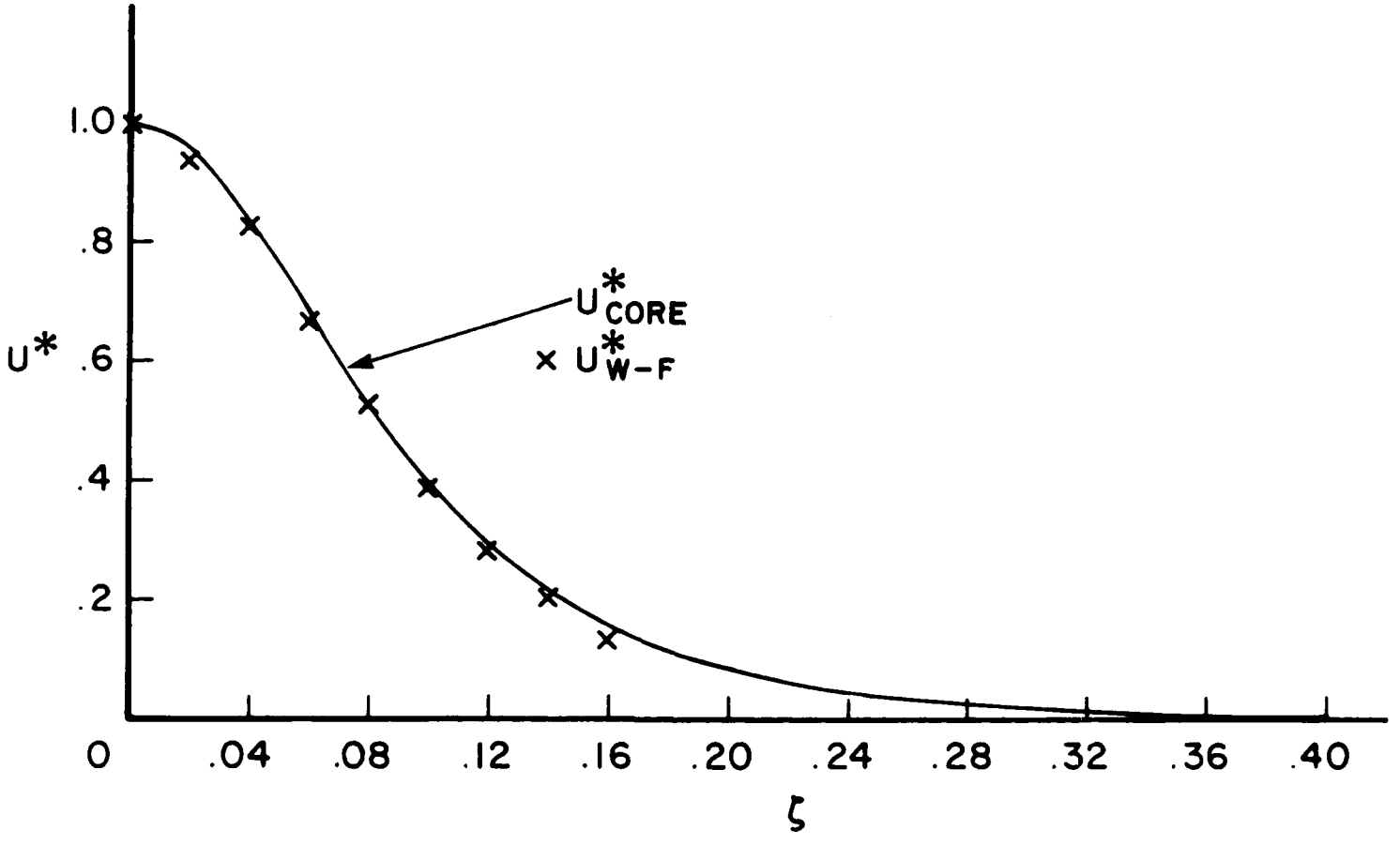

Figure 2a. Comparison with mean-velocity data of Wygnanski & Fiedler (1969).

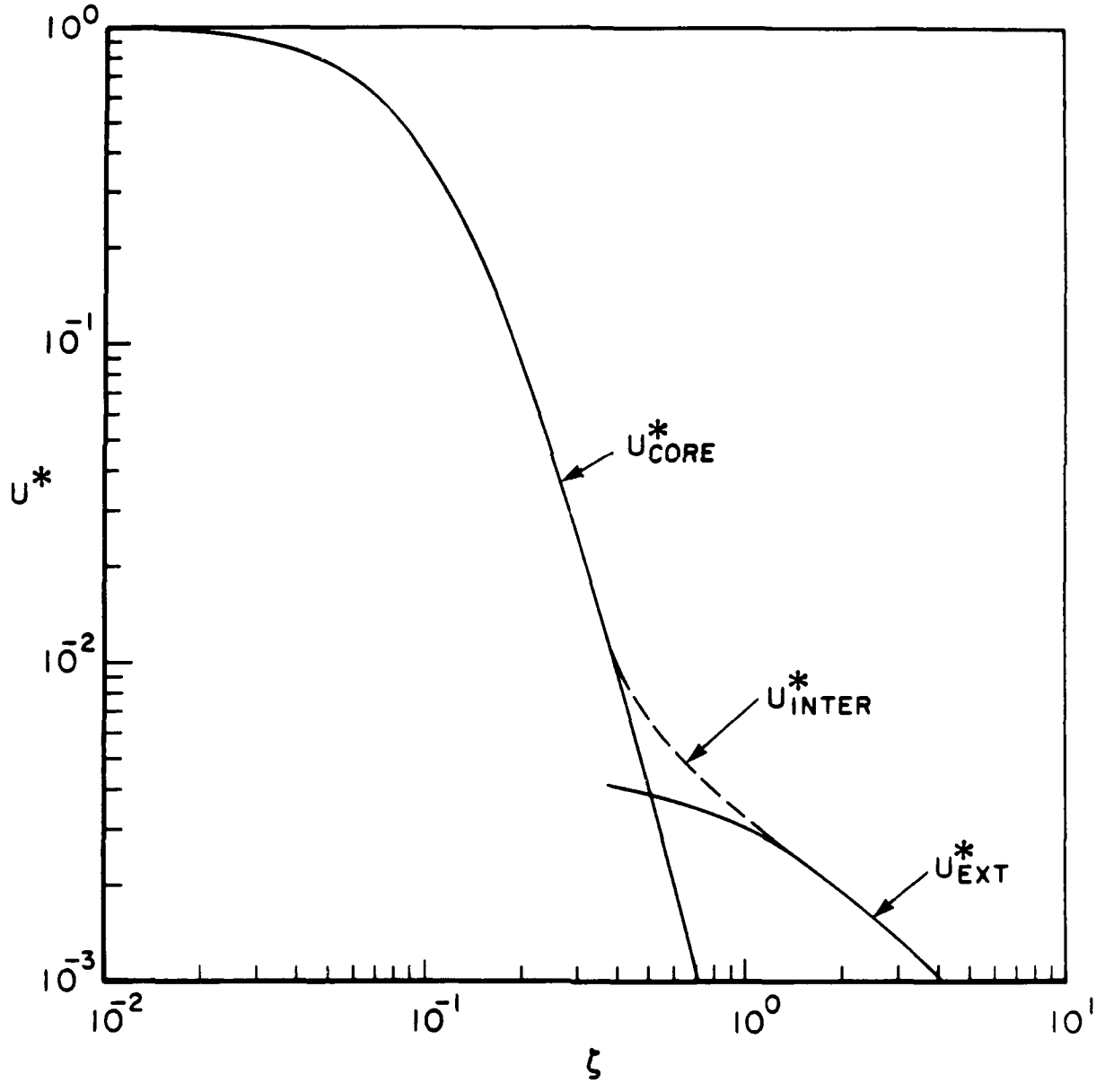

Figure 2b. Core-, intermediate-, and exterior-region mean-velocity prediction.

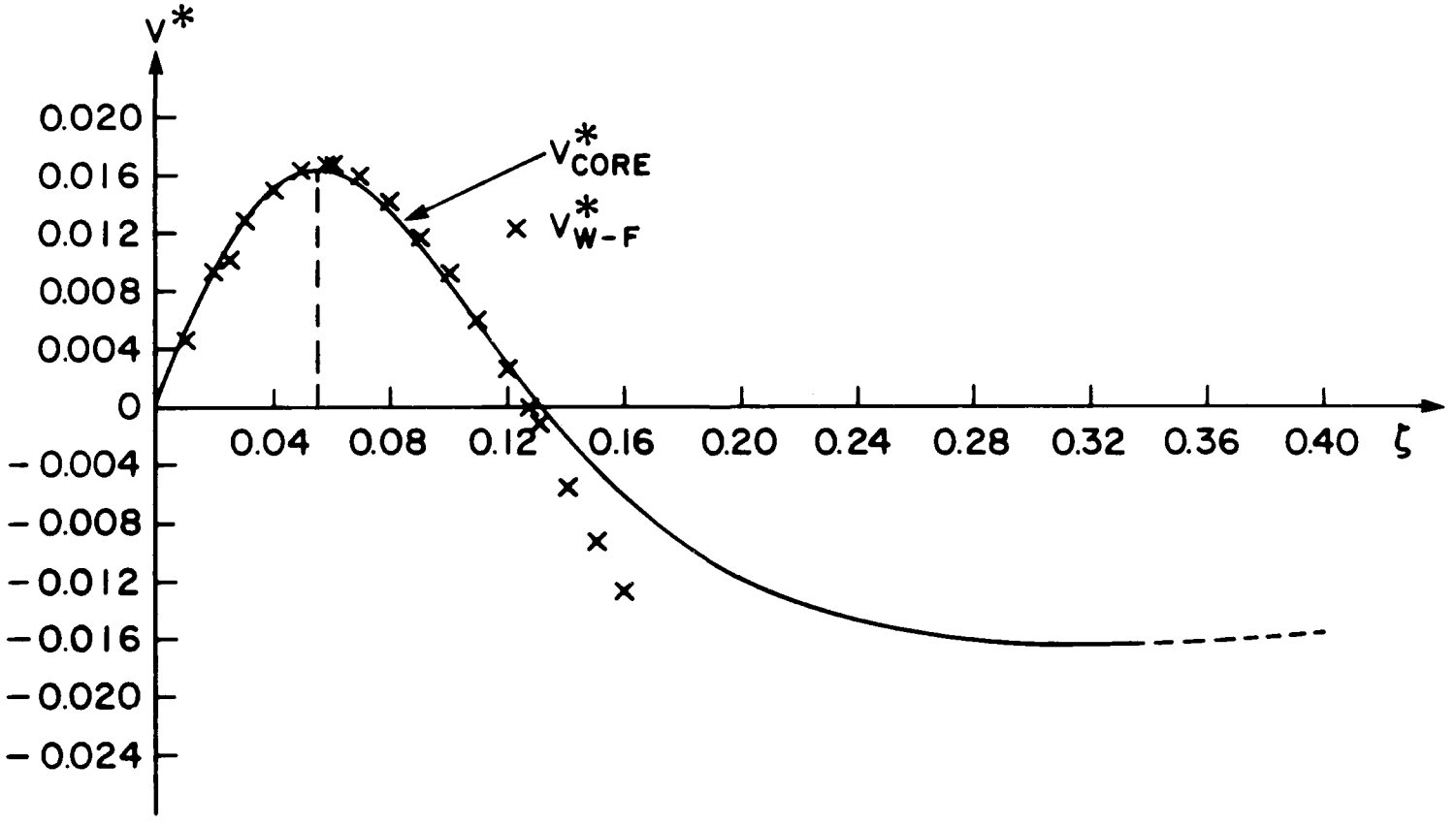

Figure 3a. Comparison of radial-velocity distribution across the jet.

are shown in figure 3b.

Since, for the core region,

$$T = -\frac{\overline{(\tilde{u}'\tilde{v}')}}{\tilde{U}_j^2} = -\overline{(u'v')} = \delta\tau = \delta\xi^{-2}\Phi,$$

the pertinent zeroth-order representation for the shear-stress distribution is

$$\Phi^* = \frac{\overline{(u'v')}}{U_{\ell}^2} \approx \frac{\zeta}{2(1 + L^2\zeta^2)^3} \equiv \Phi^*_{CORE}(\zeta; L). \tag{6.10}$$

This is essentially the relation for the shear-stress distribution employed by Hinze(1975). For the exterior region,

$$T = -\frac{\overline{(\tilde{u}'\tilde{v}')}}{\tilde{U}_j^2} = -\overline{(u'v')} = \delta^4\tau_s = \delta^4\xi^{-2}\Phi_s,$$

and the corresponding zeroth-order shear-stress distribution is

$$\Phi^* = \frac{\overline{(u'v')}}{U_{\ell}^2} \approx \frac{(4L^2)^{-2}[(1 + \zeta^2)^{1/2} + 1]}{\zeta(1 + \zeta^2)} \equiv \Phi^*_{EXT}(\zeta; L),$$

$$\text{with } (4L^2)^{-2} \approx 0.0000187 \text{ for } L^2 \approx 57.8. \tag{6.11}$$

In figure 4a, $\Phi^*_{CORE}(\zeta; L)$, of (6.10), is compared with the data of W-F, with good results. Figure 4b displays the solutions $\Phi^*_{CORE}(\zeta; L)$, $\Phi^*_{EXT}(\zeta; L)$, and $\Phi^*_{INTER}(\zeta; L)$.

For the core region, the normal-stress components are

$$M = -\frac{\overline{(\tilde{u}'^2)}}{\tilde{U}_j^2} = -\overline{(u'^2)} = \delta\mu = \delta\xi^{-2}J,$$

$$N = -\frac{\overline{(\tilde{v}'^2)}}{\tilde{U}_j^2} = -\overline{(v'^2)} = \delta\nu = \delta\xi^{-2}K,$$

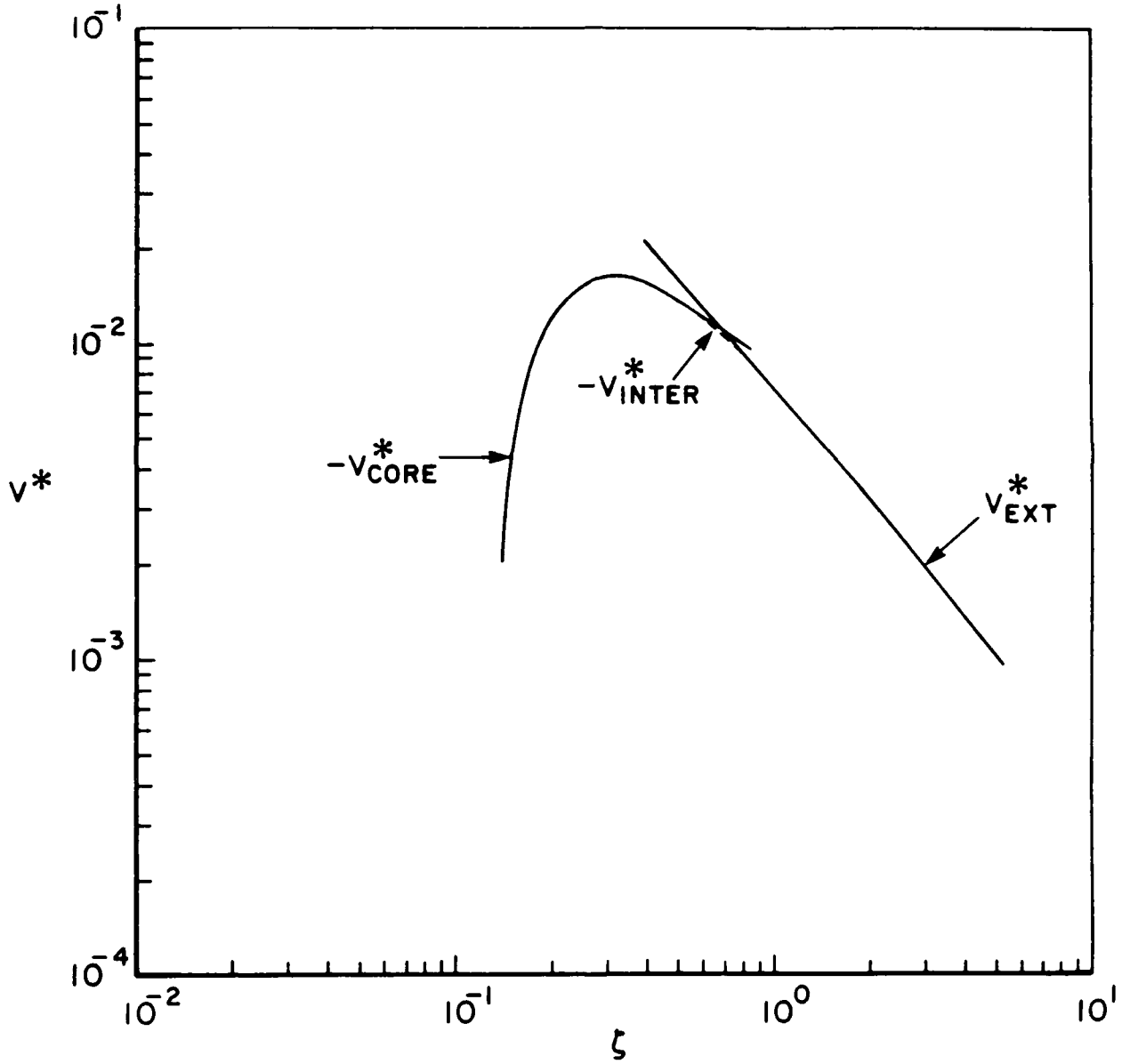

Figure 3b. Core-, intermediate-, and exterior-region radial-velocity results.

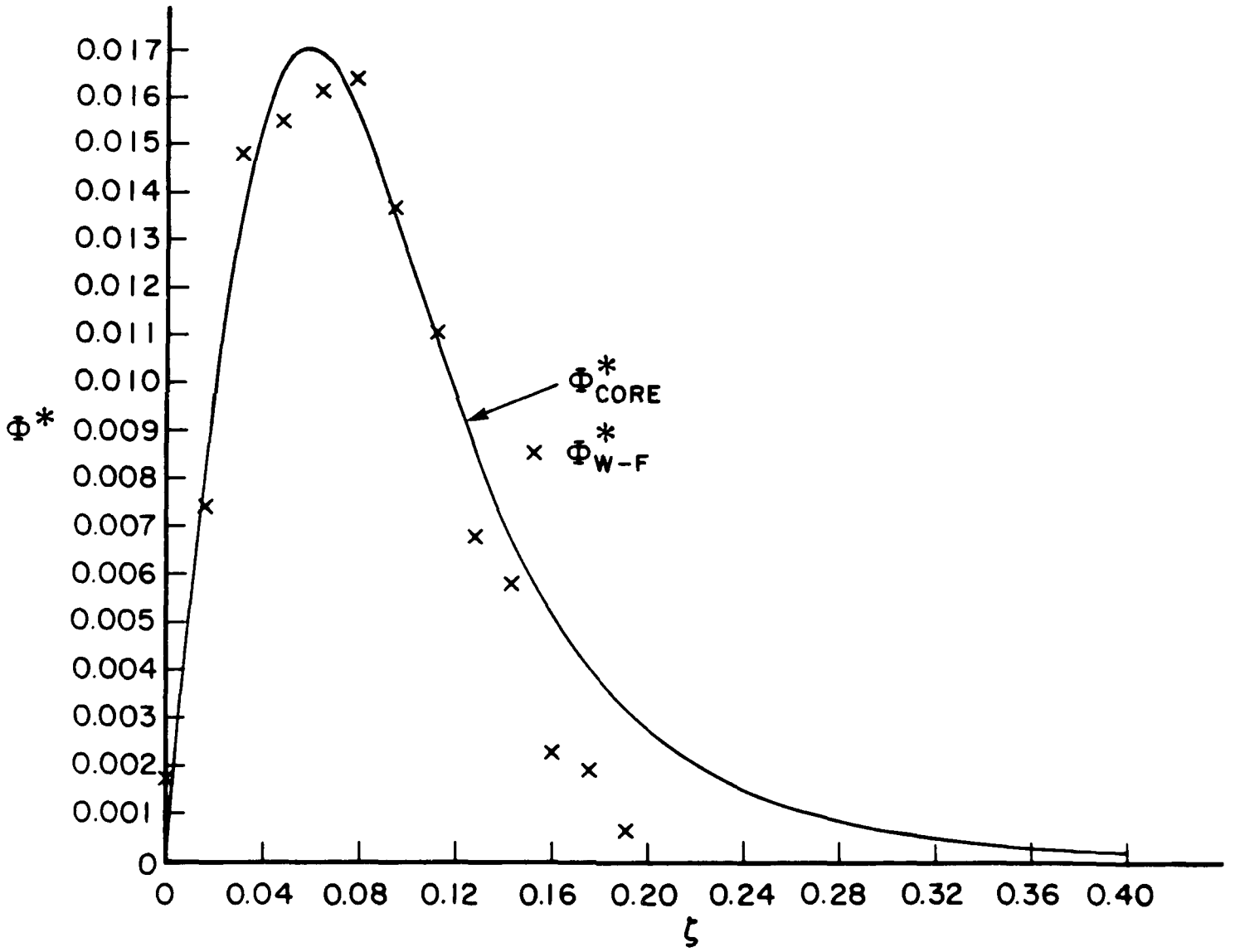

Figure 4a. Comparison of shear-stress distribution across the jet.

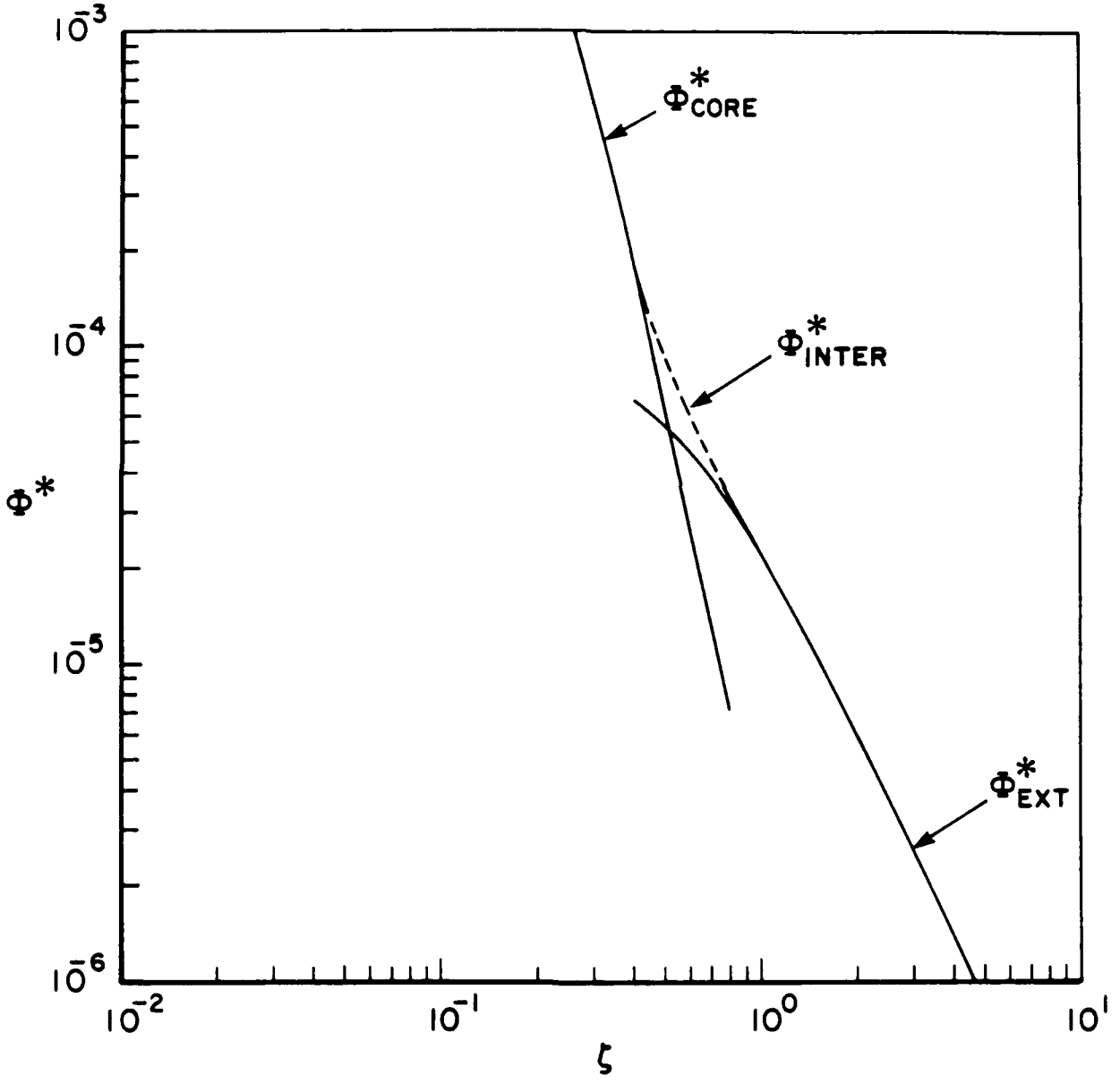

Figure 4b. Core-, intermediate-, and exterior-region shear-stress predictions.

where, at the very least, the zeroth-order approximations/models, J_o, and K_o, employed in the analysis presented in § 3, require the specification of the centerline values, a_o and b_o, respectively. The data of W-F, in conjunction with these zeroth-order models, lead to the normal-stress distributions

$$\frac{\left[\overline{(u'^2)}\right]^{1/2}}{U_{\ell}} \approx \frac{(\delta a_o)^{1/2}}{(1+L^2\zeta^2)}, \quad \frac{\left[\overline{(v'^2)}\right]^{1/2}}{U_{\ell}} \approx \frac{(\delta b_o)^{1/2}}{(1+L^2\zeta^2)},$$

$$\text{with } (\delta a_o)^{1/2} \approx 0.29, \ (\delta b_o)^{1/2} \approx 0.25. \tag{6.12}$$

From (6.12), $(\delta a_o) \approx 0.084$, $(\delta b_o) \approx 0.063$: $a_o \approx 0.98$, $b_o \approx 0.73$ for $\delta \approx 0.086$, and, in turn,

$$\begin{aligned} &(\delta B_1) \approx -0.079: \quad B_1 \approx -0.92 \text{ for } \delta \approx 0.086, \\ &(\delta A_1) = A_o(\delta B_1) \approx -0.095: \quad A_1 \approx -1.1 \text{ for } \delta \approx 0.086, \ Z \approx 0.78. \end{aligned} \tag{6.13}$$

The evaluation of (δB_1) follows directly from the normal-stress data/model comparison, without the specification of δ. Thus, it is consistent to employ $(\delta B_1) \approx -0.079$ to evaluate δ, as is done in (6.3).

ACKNOWLEDGMENT

The research reported herein was supported in part by the United States Air Force Office of Scientific Research under Contract No. F49620-88-C-0040 (Major James M. Crowley, Project Monitor).

7. REFERENCES

ABRAMOVICH, G. N. 1963. *The Theory of Turbulent Jets* (trans. by Scripta Technica; techn. ed. L. H. Schindel). Cambridge, Mass.: M. I. T. Press.

HINZE, J. O. 1975. *Turbulence* (2nd ed.). New York: McGraw-Hill.

HINZE, J. O. & VAN DER HEGGE ZIJNEN, B. G. 1949. Transfer of heat and matter in the turbulent mixing zone of an axially symmetric jet. *Appl. Sci. Res.* 1A, 435.

LANDAU, L. D. & LIFSHITZ, E. M. 1959. *Fluid Mechanics. Course of Theoretical Physics* 6. London: Pergamon Press.

REICHARDT, H. 1941. Gesetzmäßigkeiten der freien Turbulenz. *Z. angew. Math. Mech.* 21, 257.

SCHLICHTING, H. 1979. *Boundary-Layer Theory* (7th ed.; trans., J. Kestin). New York: McGraw-Hill.

TOLLMIEN, W. 1926. Berechnung turbulenter Ausbreitungsvorgänge. *Z. angew. Math. Mech.* 6, 468.

TOWNSEND, A. A. 1976. *The Structure of Turbulent Shear Flow* (2nd ed.). Cambridge University Press.

WYGNANSKI, I. & FIEDLER, H. 1969. Some measurements in the self-preserving jet. *J. Fluid Mech.* 38, 577.

APPENDIX B

FAST ALGORITHM DEVELOPMENT FOR LARGE-EDDY SIMULATION OF CIRCULAR-JET TURBULENCE: COMPUTATIONAL CONSIDERATIONS

C. A. Hall, T. A. Porsching, M. Raymund

Institute for Computational Mathematics and Applications
Department of Mathematics and Statistics
University of Pittsburgh
Pittsburgh, PA 15260

ABSTRACT

This report deals with three major computational topics associated with the numerical simulation of circular-jet flows. The first is the development of a theory surrounding the construction of hybrid differnce methods that preserve weak but persistent unsteady features of the flow. The second is a theoretical and numerical study of a classic plane jet problem as a means of deducing the nature of far-field boundary conditions. The third is a description of the algorithms underlying the "dual variable" method for the numerical simulation of three dimensional, incompressible flows.

Table of Contents

CHAPTER 1

WEIGHT SELECTION PROCEDURES FOR HYBRID DIFFERENCE METHODS

1. Introduction

To preserve weak but persistent features of an unsteady flow (such as the shedding of certain vortex structures) during numerical simulations it is necessary to use difference methods with small numerical dissipation. Unfortunately, in the absence (or near absence) of naturally occurring dissipative mechanisms, it is precisely the numerical viscosity that stabilizes the method. Thus, it is important to examine the prospect of constructing methods that are robust (with respect to their stability characteristics), but not uniformly overly dissipative.

A conceptually simple way to attentuate the dissipative effects of a difference method is to create a hybrid method by blending the given method with a less robust but more accurate one. The idea is to design the weights used in the blending process so that in regions where little numerical dissipation is needed, the accurate method is dominant, whereas in regions requiring significant numerical dissipation to preserve stability (or certain qualitative features of the solution such as monotonicity), the original scheme prevails. Such self-adjusting methods in computational fluid dynamics were apparently first considered by Harten and Zwas [1972], and a comprehensive account of the steps involved in the design of these methods is contained in the thesis of Wilders [1983].

Hybridization is also the notion behind the Flux Corrected Transport (FCT) schemes of Boris and Book [1973, 1976] and Book, Boris, and Hain [1975]. The FCT schemes, originally developed for one space dimension, were given a nontrivial multidimensional generalization by Zalasek [1979]. He also showed that they could be interpreted in terms of convex combinations of flux terms related to low-order (strongly dissipative) and high-order (marginally dissipative) difference methods. The FCT weight selection process uses a "monotonicity constraint" on the numerical solution and has a particularly simple formulation in one dimension. Specifically, the weights are determined so as to maximize the effect of the high-order method's flux terms, subject to the condition that over any timestep no extrema are introduced that would not also be present in the low-order solution at the new time. This implies that the total variation of the hybrid grid function does not exceed that of the low-order grid function. The same idea has been used to define total-variation-diminishing

(TVD) schemes (Harten [1983], [1984]).

The monotonicity constraint is consistent with the behavior of a solution for the one-dimensional scalar convection equation (the total variation of such a solution does not increase in time), and in this case the FCT algorithms perform impressively. However, the situation is different for systems of nonlinear conservation laws. According to Woodward and Colella [1984]:

> Then no such monotonicity constraint is implied by the differential equations, and the use of such a constraint can lead to difficulties. In particular, a smooth region with strong gradients can be turned into a sequence of discontinuous jumps, with the appearance of a staircase.

The unsuitability of a TVD condition in the design of difference methods for multidimensional quasilinear systems is also indicated by a result of Rauch [1986]. There it is shown that unless the commutators of all of the Jacobian matrices appearing in the system vanish, no multiple of the $W^{1,1}$ seminorm of the initial condition can bound this seminorm at a later time. Thus, it is unlikely that a numerical solution with a TVD property will converge to a solution of the original system.

In view of these difficulties with the TVD condition, it is appropriate to consider other weight selection criteria. One such alternative is based on the ability of the hybrid method to conserve (or nearly conserve) the discrete energy of the numerical solution that it produces.

In this chapter we study such hybrid difference methods for the linear convection equation,

$$u_t + a(x)u_x = 0\ ,\ 0 \le x \le 1\ ,\ t \ge 0\ , \tag{1.1}$$

subject to the initial condition,

$$u(x,0) = \psi(x). \tag{1.2}$$

We assume that $\psi \in C^1(-\infty,\infty)$ and that $a(x)$ is continuous and satisfies $\mu \ge a(x) > 0$ for some constant μ Since a hydrid method is obtained by forming weighted combinations of the differences quotients that define two consistent methods, our main concern is with the selections of the weight used in the blending process.

2. The Continuous Energy

Since we shall base our weight selection principles on the manner in which the energy of a hybrid method conforms to that of (1.1), we begin with an examination of the latter.

We first note that by using the method of characteristics, we may write the exact solution of (1.1), (1.2) as

$$u(x, t) = \psi(y(x, t)) , \tag{2.1}$$

where $y = y(x, t)$ satisfies the equation

$$\int_y^x \frac{ds}{a(s)} = t . \tag{2.2}$$

If we define the energy of (1.1) as

$$I(t) \equiv [\int_0^1 u^2(x, t)\, dx]^{1/2} ,$$

then it is clear from (2.1), that $I(t)$ is bounded when ψ is. However, it is also possible for $I(t)$ to remain bounded when ψ is not bounded.

Theorem 2.1: If $\psi\psi' \geq 0$, then $\frac{dI^2}{dt} \leq 0$.

Proof:

$$\frac{dI^2}{dt} = \int_0^1 \frac{\partial}{\partial t}(u^2)dx = 2\int_0^1 uu_t\, dx = -2\int_0^1 a(x)uu_x$$

$$= -2\int_0^1 a(x)\psi(y)\psi'(y)y_x\, dx = -2\int_0^1 a(y)\psi(y)\psi'(y)\, dy \leq 0 .$$

□

Difference methods for (1.1), (1.2) are frequently analyzed under the assumption that the corresponding numerical solution is periodic in the discrete space variable. Therefore, it is of interest to know under what conditions this is true of $u(x, t)$.

Theorem (2.2): Let ψ be an ι–periodic function. Then u is ι–periodic in x, if and only if a is ι-periodic.

Proof: If $u(x + \iota, t) = u(x, t)$, then by (2.1) $y(x + \iota, t) = y(x, t) + \iota$. Thus, by (2.2)

$$\int_{y(x,t)+\iota}^{x+\iota} \frac{ds}{a} = \int_{y(x+\iota,t)}^{x+\iota} \frac{ds}{a} = t = \int_{y(x,t)}^{x} \frac{ds}{a} ,$$

and so

$$\int_x^{x+\iota} \frac{ds}{a} = \int_y^{y+\iota} \frac{ds}{a} .$$

Differentiating this equation with respect to t, we get

$$0 = y_t \left[\frac{1}{a(y+\iota)} - \frac{1}{a(y)} \right] .$$

Since $y_t = -a(y) \neq 0$, we have $a(y+\iota) = a(y)$.

Conversely, if $a(s+\iota) = a(s)$, then

$$\int_x^{x+\iota} \frac{ds}{a}$$

is independent of x and the above steps are reversible.

□

Now we assume that ψ and a are ι-periodic. In general the energy $I(t)$ is not conserved even though $u(\cdot, t)$ is periodic. However, with regard to the weighted energy

$$J(t) \equiv [\int_0^{\iota} \frac{u^2(x,t)}{a(x)} \, dx]^{1/2} ,$$

we see that

$$\frac{dJ^2}{dt} = \int_0^{\iota} \frac{2}{a} u u_t \, dx = -\int_0^{\iota} 2 u u_x \, dx \tag{2.3}$$

$$= -\int_0^{\iota} \frac{\partial}{\partial x}(u^2) dx = 0 ,$$

so that this quantity is conserved. Moreover, since $J(0) = J(t) \geq \mu^{-1/2} I(t)$, it follows that in the case of periodicity, $I(t)$ is bounded by $[\mu \int_0^{\iota} \frac{\psi^2}{a} \, dx]^{1/2}$.

3. Hybrid Methods

Consider a rectangular mesh with uniform x and t spacings h and τ. Let v be a mesh function whose value at the mesh point $(jh, m\tau)$ is denoted by $v_j(m)$. When no confusion can arise we shall omit writing the dependence on j and/or m.

For any such function v we define the familiar x-directional differences:

$$S_x^{\pm} v = v_{j\pm1},$$

$$\Delta_x v = (v_{j+1} - v_j)/h \ ,$$

$$\nabla_x v = (v_j - v_{j-1})/h \ ,$$

$$\bar{\Delta}_x v = (v_{j+1} - v_{j-1})/2h \ ,$$

$$\delta_x^2 v = (v_{j+1} - 2v_j + v_{j-1})/h^2 \ ,$$

as well as analogous differences in the t-direction. We also note the following useful identities for any mesh functions u and v:

$$\nabla_x(u\Delta_x v) = u\delta_x^2 v + (\nabla_x u)\nabla_x v \ , \tag{3.1}$$

$$\nabla_x(uv) = u\nabla_x v + (S^- v)\nabla_x u \ , \tag{3.2}$$

$$2v\nabla_x v = \nabla_x v^2 + h(\nabla_x v)^2 \ , \tag{3.3}$$

and

$$2v\Delta_t v = \Delta_t v^2 - \tau(\Delta_t v)^2 \ . \tag{3.4}$$

With this notation we consider the following difference equation for (1.1):

$$\Delta_t v + \alpha[(1-\theta)\nabla_x v + \theta\,\bar{\Delta}_x v] = 0 \ , \tag{3.5}$$

where $\alpha_j(m) = \alpha_j = a(jh)$ and θ is a mesh function of weights. Equation (3.5) defines a consistent explicit method for any choice of θ and reduces to the "upwind" or "centered" difference method when $\theta_j(m)$ is respectively 0 or 1.

To study the energy of (3.5) (and close the system of difference equations), we assume that v is L-

periodic in j, i.e., $v_{j+L}(m) = v_j(m)$. In view of Theorem 2.2 this assumption is certainly consistent with t-periodicity in a and ψ when $h = t/L$. Now we observe that (3.5) may be rewritten as

$$\Delta_t v + \alpha(\nabla_x v + \frac{1}{2}\theta h\ \delta_x^2 v) = 0. \tag{3.6}$$

In this form the equation clearly reveals its "antidiffusive" nature when $\theta > 0$. If we use (3.1) to transform the term $\frac{\theta h}{2}\ \delta_x^2 v$ and then multiply the result by $2v/\alpha$, we get,

$$\frac{2v\,\Delta_t v}{\alpha} + 2v\nabla_x v + hv\nabla_x(\theta\Delta_x v) - h(\nabla_x\theta)v(\nabla_x v) = 0. \tag{3.7}$$

Next we use (3.4), (3.3) and (3.2) to transform the first three terms of (3.7). Upon rearranging, we have

$$\frac{\Delta_t v^2}{\alpha} + \nabla_x(v^2 + h\theta v\,\Delta_x v) \tag{3.8}$$

$$= \frac{\tau}{\alpha}(\Delta_t v)^2 + hS_x^-(\theta\Delta_x v)\nabla_x v - h(\nabla_x v)^2 + h(\nabla_x\theta)v(\nabla_x v).$$

We add $h\nu(\nabla_x v)^2$ to both sides of (3.8), where ν is a constant and observe that $S_x^-(\theta\Delta_x v)\nabla_x v = (S_x^-\theta)(\nabla_x v)^2$. In this way we obtain

$$\frac{\Delta_t v^2}{\alpha} + \nabla_x(v^2 + h\theta v\,\Delta_x v) + h\nu(\nabla_x v)^2 \tag{3.9}$$

$$= \frac{\tau}{\alpha}(\Delta_t v)^2 - h(1-\nu-S^-\theta)(\nabla_x v)^2 + h(\nabla_x\theta)(v\nabla_x v).$$

Letting

$$b = h\nabla_x\theta\ , \tag{3.10}$$

and

$$Q = \frac{\tau}{\alpha}(\Delta_t v)^2 - h(1 - \nu - S^-\theta)(\nabla_x v)^2\ , \tag{3.11}$$

we see that

$$\frac{\Delta_t v^2}{\alpha} + \nabla_x(v^2 + h\theta v\,\Delta_x v) + h\nu(\nabla_x v)^2 = Q + bhv\nabla_x v\ . \tag{3.12}$$

If we define the weighted energy of the method (3.5) as

$$\tilde{J}(m) = \left[\sum_{j=0}^{L} \frac{v_j^2(m)}{\alpha_j} h\right]^{1/2},$$

then under suitable conditions, we can use (3.12) to establish the bounded nature of $\tilde{J}$ and therefore also the boundedness of the energy

$$\tilde{I}(m) = \left[\sum_{j=0}^{L} v_j^2(m) h\right]^{1/2}.$$

These "suitable conditions" lead directly to various algorithms for the weights θ.

4. Global Weights

We assume that θ is independent of the space index j. In this case $b = 0$, and if we choose $\nu = 0$, then (3.12) reduces to

$$\frac{\Delta_t v^2}{\alpha} + \nabla_x (v^2 + h\theta v \Delta_x v) = Q \ , \tag{4.1}$$

where

$$Q = \frac{\tau}{\alpha}(\Delta_t v)^2 - h(1-\theta)(\nabla_x v)^2 \ . \tag{4.2}$$

If we multiply (4.1) by $h\tau$, sum over $0 \le j \le L$, $0 \le n \le m$, use the periodicity of v, and note that

$$\sum_{j,n} \frac{\Delta_t v^2}{\alpha} h\tau = \tilde{J}^2(m+1) - \tilde{J}^2(0) \ ,$$

we see that

$$\tilde{J}^2(m+1) = \tilde{J}^2(0) + \sum_{j,n} Qh\tau \ . \tag{4.3}$$

Hence the weighted energy is conserved if

$$\sum_{j,n} Qh\tau = 0 \ . \tag{4.4}$$

To enforce (4.4) we observe that by (3.6),

$$Q/h = \lambda[\nabla_x v + \frac{1}{2}\theta h \delta_x^2 v]^2 - (1-\theta)(\nabla_x v)^2 , \tag{4.5}$$

where $\lambda \equiv \tau\alpha/h$ is the mesh function of Courant numbers. Thus

$$\sum_j Qh\tau = (A\ \theta^2 + B\theta + C)h^2\tau ,$$

where

$$\begin{cases} A = \dfrac{h^2}{4}\sum_j \lambda(\delta_x^2 v)^2 , \\ B = \sum_j [\lambda h \delta_x^2 v + \nabla_x v]\nabla_x v , \\ C = \sum_j (\lambda - 1)(\nabla_x v)^2 . \end{cases} \tag{4.6}$$

Therefore, (4.4) follows if θ is a real root of the quadratic equation.

$$q_2(\theta) \equiv A\ \theta^2 + B\theta + C = 0 . \tag{4.7}$$

If the "Courant condition", $\lambda \le 1$ holds, then

$$q_2(0) = \sum_j (\lambda - 1)(\nabla_x v)^2 \le 0 ,$$

and

$$q_2(1) = \sum_j \lambda\,(\bar{\Delta}_x v)^2 \ge 0 .$$

Hence (4.7) has a root in the interval [0,1].

If we insist that θ also be independent of the time index m (i.e. θ = *constant*), then we cannot in general satisfy (4.4). However, if we write (4.5) in the form

$$Q/h = \lambda[(1 - \frac{1}{2}\theta)\nabla_x v + \frac{1}{2}\theta\Delta_x v]^2 - (1-\theta)(\nabla_x v)^2 ,$$

let $\Lambda = \mu\,\tau/h$, and use the elementary inequality $(a+b)^2 \le 2(a^2+b^2)$, then we do have

$$Q/h \le \Lambda[(1 - \frac{1}{2}\theta)\nabla_x v + \frac{1}{2}\theta\Delta_x v]^2 - (1-\theta)(\nabla_x v)^2$$

$$\le [2\Lambda(1-\frac{1}{2}\theta)^2 + \theta - 1](\nabla_x v)^2 + \frac{1}{2}\Lambda\theta^2(\Delta_x v)^2 .$$

Therefore, using the periodicity of v, we see that

$$\sum_j Qh\tau \le q_1(\theta) \sum_j (\nabla_x v)^2 h^2 \tau ,$$

where

$$q_1(\theta) \equiv \Lambda\theta^2 + (1-2\Lambda)\theta + 2\Lambda - 1 . \tag{4.8}$$

From (4.3) we conclude that if θ is a real root of $q_1(\theta) = 0$, then the weighted energy, is bounded for all m. Note that if $\Lambda \le \frac{1}{2}$, then $q_1(0) \le 0 \le q_1(1)$, and so there is a root in [0,1].

We summarize our findings as follows.

Theorem 4.1: If $\Lambda = \mu\tau/h \le \frac{1}{2}$ and

$$\theta = \frac{2\Lambda - 1 + (1-4\Lambda^2)^{1/2}}{2\Lambda} , \tag{4.9}$$

then the weighted energy $\tilde{J}$ of the hybrid method (3.5) satisfies $\tilde{J}(m) \le \tilde{J}(0)$ for all $m \ge 0$.

□

Theorem 4.2: If $\lambda = \tau\alpha/h \le 1$, and $\theta(m)$ is the root of

$$A(m)\theta^2 + B(m)\,\theta + C(m) = 0 , \tag{4.10}$$

lying in [0,1], where

$$\begin{cases} A(m) = \dfrac{h^2}{4} \displaystyle\sum_j \lambda_j(m)\,(\delta_x^2 v_j(m))^2, \\ B(m) = \displaystyle\sum_j [h\lambda_j(m)\delta_x^2 v_j(m) + \nabla_x v_j(m)]\,\nabla_x v_j(m), \\ C(m) = \displaystyle\sum_j (\lambda_j(m) - 1)(\nabla_x v_j(m))^2, \end{cases} \tag{4.11}$$

then the weighted energy of (3.5) is conserved, i.e,

$$\tilde{J}(m) = \tilde{J}(0) \quad \text{for all } m \ge 0 .$$

□

5. Local Weights

We now allow θ to depend on both j and m. To bound the weighted energy in this case we use a technique of Ladyzhenskaya [1985].

We choose $\nu > 0$, multiply (3.12) by $h\tau$, and sum over $0 \le j \le L$, $0 \le n \le m$. Upon simplification, the result is

$$\tilde{J}^2(m+1) + h\nu \sum_{j,n} (\nabla_x v)^2 h\tau = \tilde{J}^2(0) + \sum_{j,n} Qh\tau + h \sum_{j,n} bv\nabla_x v \; h\tau, \tag{5.1}$$

where b and Q are given by (3.10) and (3.11). Now assume that $|b| \le \mu$ and

$$\sum_{j,n} Qh\tau \le 0 . \tag{5.2}$$

Then,

$$\tilde{J}^2(m+1) + h\nu \sum_{j,n} (\nabla_x v)^2 h\tau \le \tilde{J}^2(0) + h\mu \sum_{j,n} |v\nabla_x v| h\tau \tag{5.3}$$

Applying Cauchy's inequality to the last term of (5.3), we have

$$\tilde{J}^2(m+1) + h\nu \sum_{j,n} (\nabla_x v)^2 h\tau \le \tilde{J}^2(0) + h\mu (\sum_{j,n} v^2 h\tau)^{1/2} (\sum_{j,n} (\nabla_x v)^2 h\tau)^{1/2} . \tag{5.4}$$

But, for any $f, g \ge 0$, $\nu > 0$, one has the inequality

$$h\mu fg \le \frac{h\nu}{2} g^2 + \frac{h\mu^2}{2\nu} f^2 ,$$

and it follows from (5.4) that

$$\tilde{J}^2(m+1) + \frac{h\nu}{2} \sum_{j,n} (\nabla_x v)^2 h\tau \le \tilde{J}^2(0) + \frac{h\mu^2}{2\nu} \sum_{j,n} v^2 h\tau . \tag{5.5}$$

$$\le \tilde{J}^2(0) + \frac{h\mu^3}{2\nu} \sum_{j,n} \frac{v^2}{\alpha} h\tau$$

$$= \tilde{J}^2(0) + \frac{h\mu^3}{2\nu} \sum_{n} \tilde{J}^2(n)\tau .$$

Let

$$y(m) = \max_{0 \le n \le m} \tilde{J}(n) .$$

Then the right side of (5.5) is majorized by

$$y(m+1)\,\tilde{J}(0) + \frac{h\mu^3}{2\nu}\, y^2(m+1)(m+1)\tau .$$

Assuming that $(m+1)\tau \le t_1$, we deduce that

$$\tilde{J}^2(m+1) + \frac{h\nu}{2} \sum_{j,n} (\nabla_x v)^2 h\tau \le y(m+1)\tilde{J}(0) + \frac{h\mu^3 t_1}{2\nu}\, y^2(m+1) . \tag{5.6}$$

This inequality in turn implies that

$$(1 - \frac{h\mu^3 t_1}{2\nu})\, y(m+1) \le \tilde{J}(0) .$$

Therefore, if $h \le h_0$ and $t_1 \le \frac{\nu}{h_0\mu^3}$, then

$$y(m+1) \le 2\tilde{J}(0) . \tag{5.7}$$

Now we fix $t < \infty$ and divide the interval $[0, t]$ into a finite number of sub-intervals, each of whose lengths does not exceed $\frac{\nu}{h_0\mu^3}$. Then the estimate (5.7) applies on each sub-interval, and we have proven the following theorem.

Theorem 5.1: Let $h \le h_0$, $h\,|\nabla_x \theta| \le \mu$ and $\nu > 0$. If (5.2) holds, then for any $t < \infty$, there is a number $K(t)$ such that for all m satisfying $m\tau \le t$,

$$\tilde{J}(m) \le K(t)\,\tilde{J}(0) .$$

□

In view of (3.11) and (3.6), it is clear that (5.2) reduces to an equality if

$$\lambda^{1/2}(\nabla_x v + \frac{\theta h}{2}\,\delta_x^2 v) = (1 - \nu - S^{-}\theta)^{1/2}(\nabla_x v), \tag{5.8}$$

where again $\lambda = \tau\alpha/h$. This is a system of nonlinear difference equations for θ which is to hold for $j = 0, \cdots, L$. However, due to the L-periodicity of λ and v, it suffices to apply it for $j = 1, \cdots, L$ and take $\theta_0 = \theta_L$.

We now examine circumstances under which (5.8) yields a scheme (3.5) that is "total-variation diminishing" (TVD). Recall that the total-variation of a L-periodic mesh function v may be defined as

$$TV(v) \equiv \sum_{k=1}^{L} |\nabla_x v_k| h \ ,$$

and the difference method

$$v_j(m+1) = \sum_k c_{jk} v_{j+k}(m) \tag{5.9}$$

is TVD if $TV(v(m+1)) \le TV(v(m))$.

We consider solutions of (5.8) that satisfy

$$1 - \nu \ge \theta_{i-1} \ge 1 - \nu - \frac{1}{\lambda_j} \ , j = 1, \cdots , L \ . \tag{5.10}$$

Note that if $\lambda_j < 1$, then (5.10) admits the possibility of negative weights.

Theorem 5.2: If the weights θ_j satisfy (5.8) and (5.10), then (3.5) is TVD.

Proof: According to (5.8), we have

$$\Delta_t v = -\alpha_k \lambda_j^{-\frac{1}{2}} (1 - \nu - \theta_{j-1})^{\frac{1}{2}} \nabla_x v_j \ .$$

Therefore,

$$v_j(m+1) = [1 - \lambda_j^{\frac{1}{2}} (1 - \nu - \theta_{j-1})^{\frac{1}{2}}] v_j(m) + \lambda_j^{\frac{1}{2}} (1 - \nu - \theta_{j-1})^{\frac{1}{2}} v_{j-1}(m) \ .$$

If (5.10) holds, then $v_j(m+1)$ is a convex combination of $v_j(m)$ and $v_{j-1}(m)$, and it follows from a result of Lax (See Harten [1984]) that (3.5) is TVD.

□

It is worth noting that the above proof also shows that

$$min\,[v_{j-1}(m), v_j(m)] \le v_j(m+1) \le max\,[v_{j-1}(m), v_j(m)].$$

Therefore, under the hypothesis of Theorem 5.2, if $v(m)$ is monotone on the index set $j_0, \cdots , j_1$, then $v(m+1)$ is monotone on $j_0+1, \cdots , j_1$.

The difficulties of solving system (5.8) may be avoided if we consider instead the *uncoupled* equations,

$$\lambda^{1/2}(\nabla_x v + \frac{\theta h}{2}\delta_x^2 v) = (1-\theta)^{1/2}\nabla_x v \ . \tag{5.11}$$

All solutions of these equations are, of course, contained in the solutions of the quadratics,

$$A\ \theta^2 + B\ \theta + C = 0, \tag{5.12}$$

where

$$\begin{cases} A = h^2\lambda(\delta_x^2 v)^2/4, \\ B = h\lambda(\nabla_x v)(\delta_x^2 v) + (\nabla_x v)^2 \\ C = (\lambda - 1)(\nabla_x v)^2. \end{cases} \tag{5.13}$$

If we determine the weights using (5.11), then we have no guarantee that Theorem 5.1 holds. However, if we have a solution of (5.11) that also satisfies

$$1 \geq \theta > 1 - \frac{1}{\lambda}\ , \tag{5.14}$$

then as in the proof of Theorem 5.2 we may again show that the resulting scheme is TVD and monotone.

Theorem 5.3: If $\lambda \leq 1$, then there is a solution of (5.11) satisfying (5.14). Consequently the corresponding difference method is TVD and monotone.

Proof: If $\nabla_x v = 0$, then we can take $\theta = 0$. If $\nabla_x v \neq 0$, and we write (5.11) in the form

$$\lambda^{1/2}(1 + p\,\theta) = (1-\theta)^{1/2}\ ,$$

where $p = h\,\delta_x^2 v/(2\nabla_x v)$, then it is easy to see (Figure 1) that (5.11) has a solution $0 \leq \theta \leq 1$ if $p \geq -1$ while if $p < -1$, then (5.11) has a solution $1 - \frac{1}{\lambda} \leq \theta \leq 0$.

□

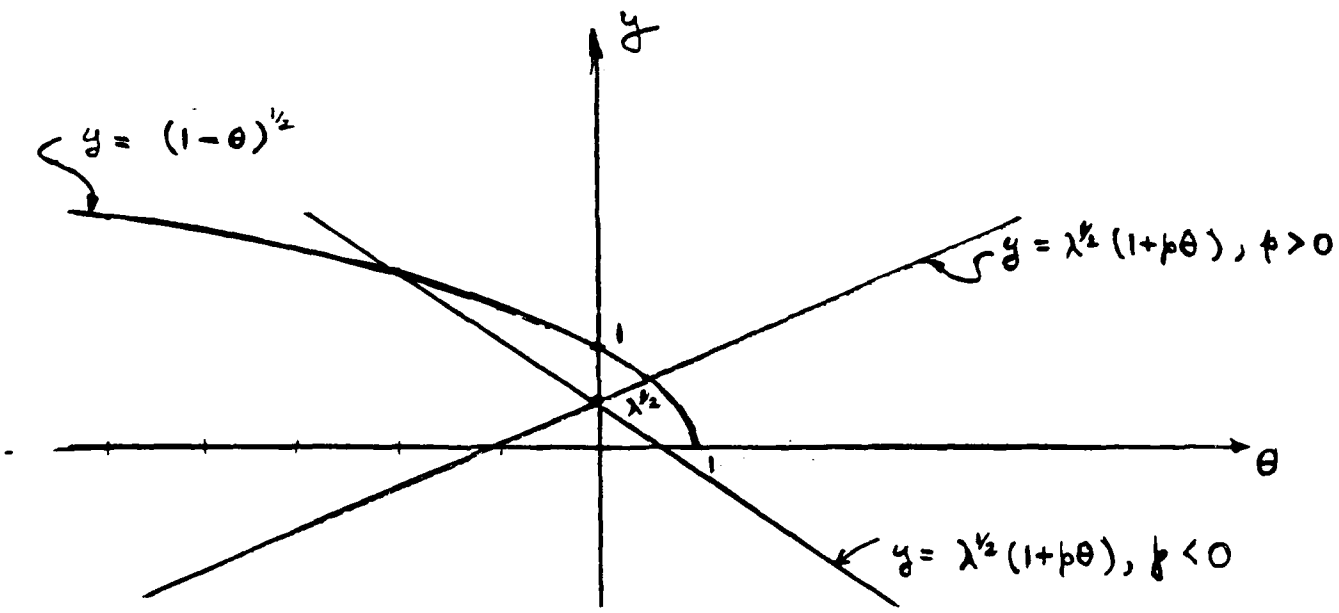

Figure 1. Solutions of (5.11)

6. Numerical Experiments

Using the results of the previous sections, we can formulate three algorithms for the determination of the weights that appear in (3.5). These algorithms, labeled Algorithms 1, 2 and 3 in increasing order of sophistication, are as follows.

Algorithm 1 (Theorem 4.1):

1. Choose $\tau < h/2\mu$.

2. $\Lambda = \mu\tau/h$.

3 $\theta = [2\Lambda - 1 + (1-4\Lambda^2)^{1/2}]/2\Lambda$.

Algorithm 2 (Theorem 4.2):

1. Choose $\tau \leq h/\mu$.

2. For $m = 0, 1, \cdots$

   Compute $A(m), B(m), C(m)$ by (4.11).

   Solve $A(m)\theta^2 + B(m)\theta + C(m) = 0$ for $\theta \in [0, 1]$.

Algorithm 3 (Theorem 5.3)

1. Choose $\tau \leq h/\mu$.

2. For $m = 0, 1, \cdots$

   For $j = 0, \ldots, L$.

   $\lambda = \tau\alpha/h$

   Compute A, B, C by (5.13).

   Solve $A\theta^2 + B\theta + C = 0$ for $\theta \in (1-1/\lambda, 1]$.

These three algorithms were used to determine the weights in a series of numerical simulations of the square wave test problems given in Boris and Book [1973]. For this problem we have $a(x) \equiv .01$ and $h = .01$. If we take $\mu = .01$, then the restrictions on τ imposed by the three algorithms are all satisfied if $\tau = .2$. This is

significantly beneath the Courant number stability limit of $\tau = 1$ that applies to the pure upwind scheme ($\theta \equiv 0$). Consequently, as time progresses, this scheme will drastically "smear" the shape of the convected wave. We note that the "exact solution" of the problem is

$$u(x, t) = \psi(x - .01t) \text{ , where}$$

$$\psi(x) = \begin{cases} 2 & \text{if } n \le x \le n + .2 \text{ , } n = 0, \pm 1, \pm 2, ..., \\ \frac{1}{2} & \text{otherwise .} \end{cases}$$

The results of the numerical experiments are shown in Figure 2 after 800 time steps ($t = 160$). For comparison, the well known (and highly dissipative) "upwind" solution is also included. The numerical solutions are shown superimposed on the exact solution. It is obvious that all three algorithms dramatically reduce the numerical dissipation of the upwind scheme. Moreover, the dispersive "ripples" of Algorithm 1 are substantially attenuated by Algorithm 2, and completely eliminated by Algorithm 3.

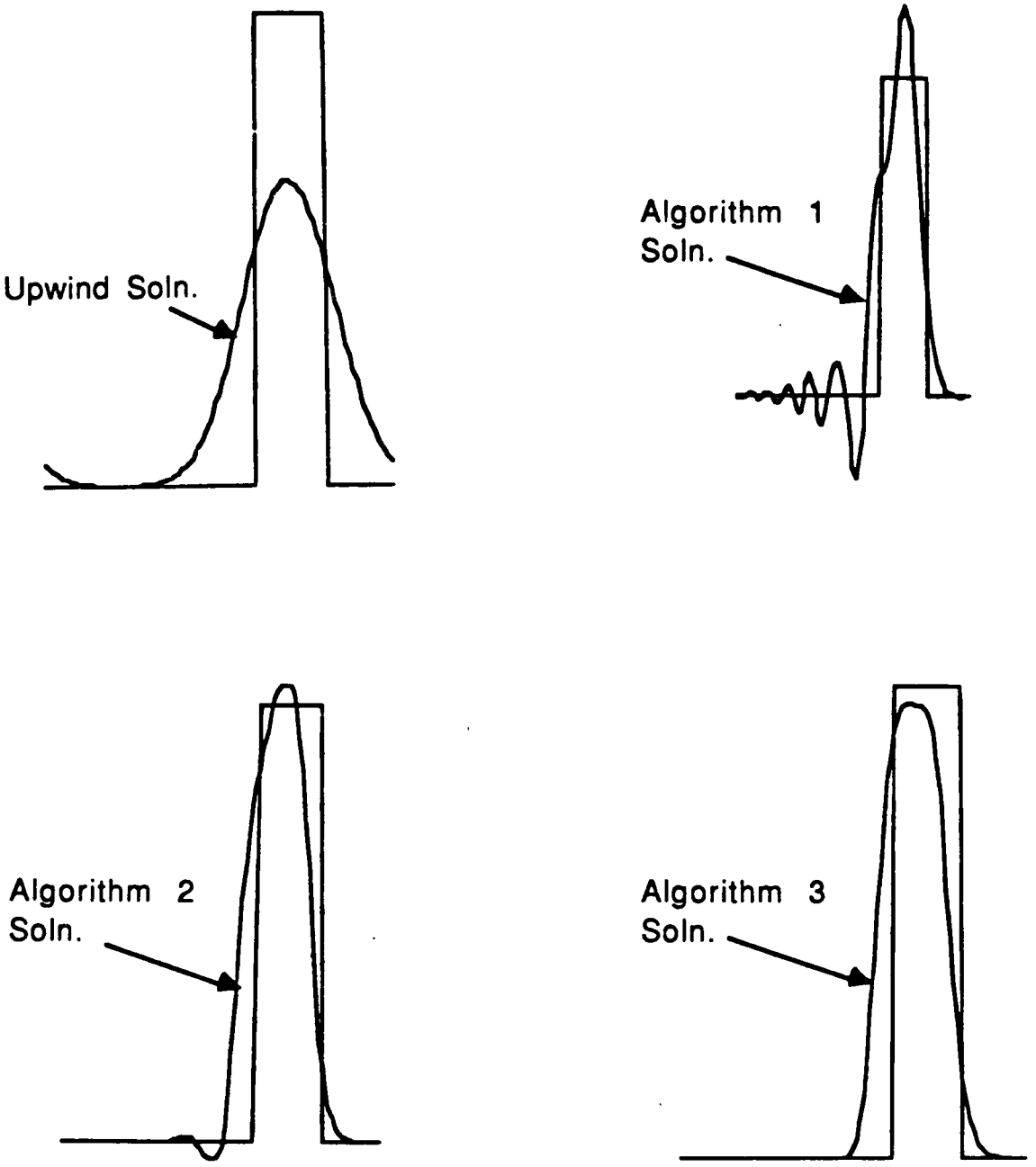

Figure 2. Hybrid Solutions.

CHAPTER 2

THEORETICAL AND NUMERICAL STUDIES OF A PLANE JET

1. Introduction

The specification of boundary conditions for the numerical computations of free-jet development presents many difficulties. The ideal configuration is that of a jet discharging into an unbounded domain. However, most numerical approaches require that the problem be transformed into a pseudo boundary-value problem on the domain of the computational grid. Thus it is necessary to impose far-field conditions on certain artifically introduced boundaries.

A typical situation is shown in Figure 1. The dashed lines represent the pseudo boundaries in the quarter plane. Of the variety of conditions tested, specification of the pressure on these boundaries appears to yield the most realistic behavior of the numerical solution. Appropriate pressure distributions may be obtained by assuming that the far-field conditions are approximately those of related model problems for which analytical solutions are known. For example, a linear distribution results from a Poiseuille flow-type assumption. Another possibility, which is the subject of this chapter, is to use the pressure field corresponding to irrotational flow of a jet with free stream lines. This is a classic problem of a type first considered by Helmholtz [1868] for the flow out of a slot (plane jet). Its solution has been reproduced in many hydrodynamics texts (see, for example, Milne-Thompson [1955]). The solution technique uses a sequence of Schwarz-Christoffel transformations to obtain an implicit representation of the complex potential of the motion. Bernoulli's theorem may then be employed to relate the far-field pressure on streamlines within the jet to the known pressure at infinity. In the next section of the Chapter we rederive the solution in a form suitable for numerical computation. Then we utilize the resulting exact far-field boundary condition to provide a setting of a problem that can be studied numerically.

2. The Plane Jet

Under certain simplifying assumptions, the motion of a plane jet issuing from an aperature in an infinitely long wall may be analytically determined. In $x-y$ geometry, the assumptions are that the motion is steady, inviscid, irrotational and incompressible.

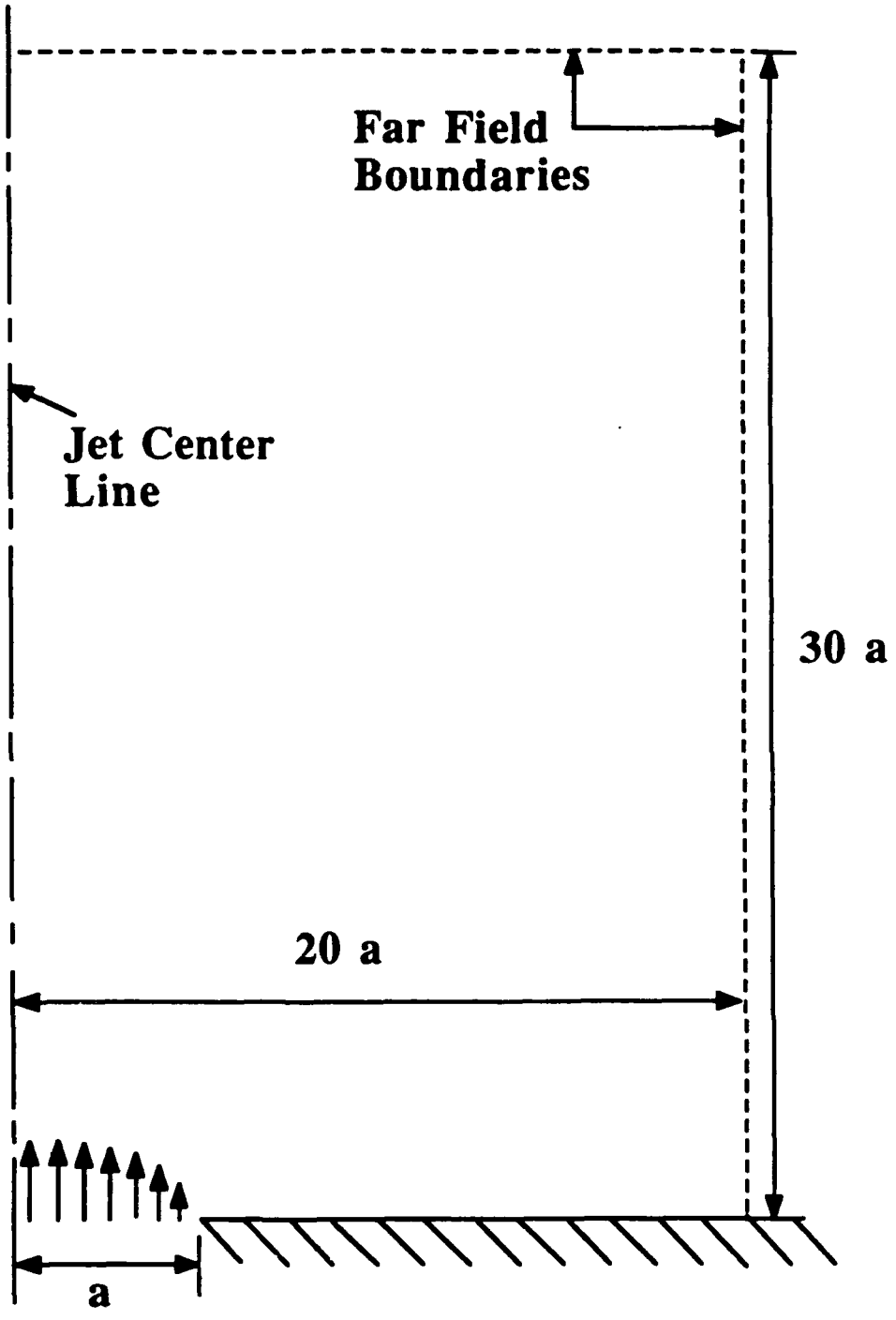

Figure 1. Problem Geometry.

With these assumptions, it is known that there is a velocity potential ϕ and a stream function ψ such that the velocity field (u,v) is given by

$$u = -\phi_x = -\psi_y \ , \tag{2.1}$$

$$v = -\phi_y = \psi_x \ . \tag{2.2}$$

Moreover, since ϕ and ψ satisfy the Cauchy-Riemann equations, they form the real and imaginary parts of an analytic function of a complex variable z. Thus if $z = x + iy$, then

$$\phi(x,y) + i\psi(x,y) \equiv w, \tag{2.3}$$

where w is some analytic function of z. The function w is called the *complex potential* of the motion. Clearly, the determination of w constitutes the solution of the problem.

The geometry of the jet problem in the complex z-plane is shown in Figure 2. There is symmetry about the streamline EF.

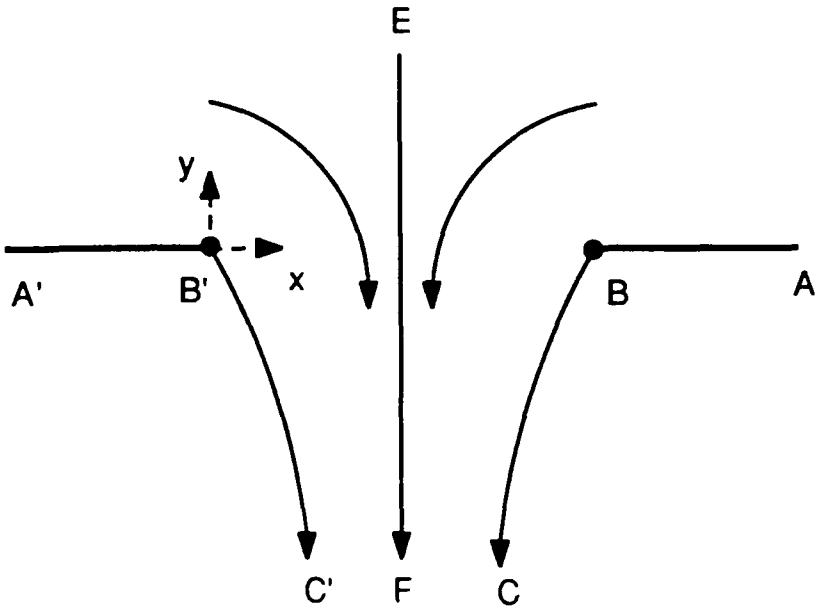

Figure 2. z-plane.

It is also assumed that the aperature width $B'B = 2a$ and that the uniform speed of the jet at $C'C$ is U. The curve ABC is a streamline of the flow and in particular the portion BC is a *free streamline*. This means that on BC (but not necessarily on AB) the speed $q \equiv (u^2+v^2)^{1/2}$ is equal to the constant U. The same is true of the curve $A'B'C'$. Since the flow is inviscid, it is possible for the fluid outside the jet to remain at rest (i.e. q is discontinuous across the free stream lines). If σ is the (unknown) *coefficient of contraction*, i.e. $\sigma = \overline{C'C}/2a$, then the efflux at $C'C$ is $2\sigma aU$. We now examine the consequences of these assumptions in the w-plane.

Since ψ is arbitrary up to an added constant, we can take $\psi = 0$ as EF. Next we note that on $C'C$, $\psi_x = v = -U$. Thus, if we denote the values of ψ at C' and C by ψ_1 and ψ_2 respectively, we have

$$(\psi_2 - \psi_1)/2\sigma a = -U \ .$$

But the conditions at E and the symmetry imply that $\psi_1 = -\psi_2$. Therefore, on the streamline $A'B'C'$, $\psi = \psi_1 = \sigma aU$ and on ABC, $\psi = \psi_2 = -\sigma aU$. Finally, we take $\phi=0$ at B (and B'). The condition $\phi_y = -v = U$ at C implies that $\phi = -\infty$ at C (and C'). Evidently, $\phi = \infty$ at A (and A'). This yields the situation shown in Figure 3.

Next we observe that

$$\frac{dz}{dw} = (\frac{dw}{dz})^{-1} = (\phi_x + i\,\psi_x)^{-1} = (-u+iv)^{-1}$$

$$= -(u-iv)^{-1} \equiv -1/\upsilon,$$

where $\upsilon = u-iv$ is the *complex velocity*. If we write this in polar form as

$$\upsilon = q\ e^{-i\theta} \ ,$$

then

$$\xi \equiv -U\ \frac{dz}{dw} = \frac{U}{\upsilon} = \frac{U}{q}\ e^{i\theta} \ . \tag{2.4}$$

Note that $u+iv = qe^{i\theta}$ so that q is the magnitude (speed) and θ the direction of the velocity vector. Now we determine how the streamlines $A'B'C'$ and ABC transform in the ξ plane. We see that:

$$A'B' \rightarrow \xi = U/q \ , \ 0 < q \le U \ .$$

$$B'C' \rightarrow \xi = e^{i\theta} \ , \ 0 \ge \theta > -\pi/2 \ .$$

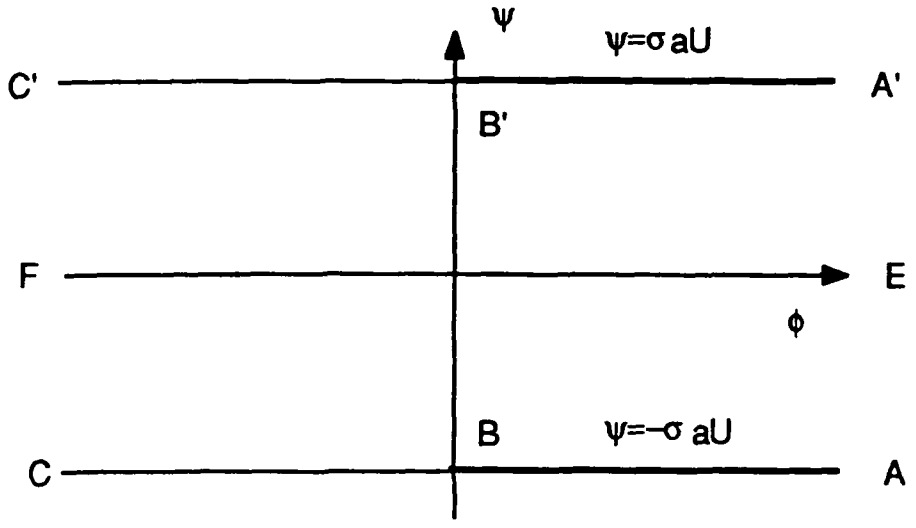

Figure 3. w-plane.

$$CB \rightarrow \xi = e^{i\theta} \quad , \quad \frac{-\pi}{2} > \theta \geq -\pi \, .$$

$$BA \rightarrow \xi = -U/q \quad , \quad U \geq q > 0 \, .$$

Thus we have the situation shown in Figure 4.

If we let

$$Q \equiv \log \xi = \log \frac{U}{q} + i\theta \, , \tag{2.5}$$

it follows from Figure 3, that in the Q-plane the streamlines of Figure 2 correspond to the curves shown in Fig

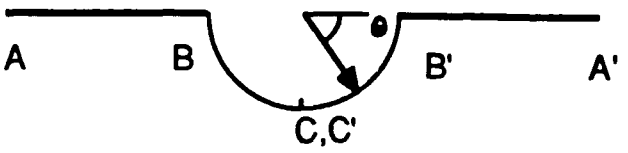

Figure 4. ξ-plane.

ure 5.

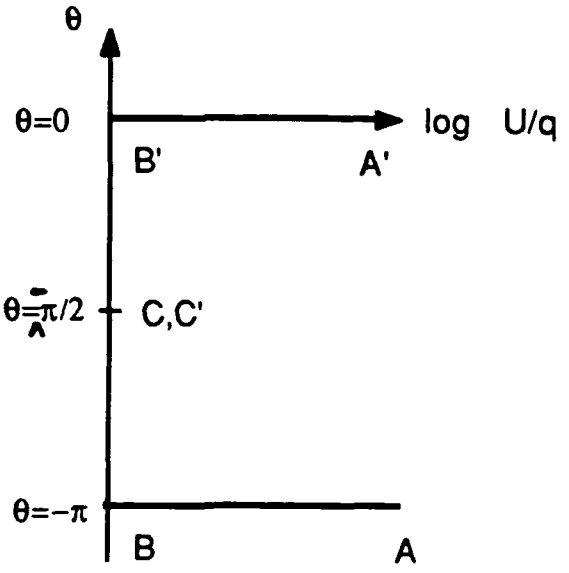

Figure 5. Q-plane.

It remains to devise Schwarz-Christoffel transformations that map respectively the interior of the "polygons" $A'B'C'CBA$ shown in Figures 3 and 5 onto the upper half of the complex ζ-plane This is easily done

using the theory of such transformations (See Milne-Thompson [1955, ch. 10]). These transformations may be constructed to produce the configuration of Figure 6.

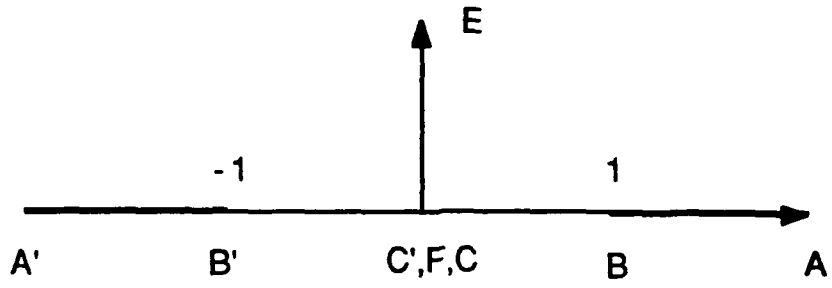

Figure 6. ζ-plane.

They are explicitly given by the formulas,

$$w = f(\zeta) = \frac{2\sigma a U}{\pi} \log \zeta - i\sigma a U \ . \tag{2.6}$$

and

$$Q = g(\zeta) = \cosh^{-1}\zeta - i\pi \ . \tag{2.7}$$

Since $i\pi = \log(-1)$, we may write (2.7) as

$$\log\left(-U\frac{dz}{dw}\right) = \log\left[\zeta+(\zeta^2-1)^{1/2}\right] - \log(-1)$$

$$= \log\left[-\zeta-(\zeta^2-1)^{1/2}\right] .$$

Therefore,

$$U\ dz = \left[\zeta + (\zeta^2-1)^{1/2}\right] dw \ . \tag{2.8}$$

If $b = \pi/2\sigma a U$, then (2.6) yields

$$\frac{dw}{d\zeta} = \frac{1}{b\zeta} \tag{2.9}$$

and

$$\zeta = ie^{bw} . \tag{2.10}$$

Combining (2.8) and (2.9), we get

$$bUdz = [1 + \frac{(\zeta^1-1)^{1/2}}{\zeta}] \, d\zeta . \tag{2.11}$$

Integrating the equation, we obtain

$$bU\int_0^z dz = \int_{-1}^{\zeta} [1 + \frac{(zet^2-1)^{1/2}}{\zeta}] \, d\zeta ,$$

which upon evaluation of the integrals gives

$$bUz = \zeta + 1 + \pi + (\zeta^2-1)^{1/2} - \cos^{-1}(1/\zeta) \tag{2.12}$$

The coefficient of contraction σ is easily determined from (2.12). Since the point B corresponds to $\zeta = 1$, we have $bU\,2a = 2+\pi$, which yields $\sigma = \pi/(\pi+2)$ in agreement with the classical theory.

To use (2.8), (2.10) and (2.12) to solve the jet problem we may proceed as follows.

(I) Use (2.12) to trace the z-plane curves corresponding to the ζ-plane rays:

$$\zeta = \rho e^{i\alpha} \quad -\pi < \alpha < \pi/2, \;\; 0 < \rho < R .$$

According to (2.10),

$$\zeta = e^{i\phi} e^{i(b\psi+\pi/2)} .$$

Therefore, the z-plane curves are the streamlines

$$\psi = (\alpha-\pi/2)/b$$

lying in the right half of Figure 2. In particular the streamline ABC corresponds to $\alpha = 0$. Note that the complex inverse cosine is given by

$$\cos^{-1}t = -i \, \log \, (t+i\,(1-t^2)^{1/2}) .$$

(II) Observe that if

$$\zeta + (\zeta^2-1)^{1/2} \equiv Re^{i\beta} ,$$

then by (2.8)

$$Re^{i\beta} = U \frac{dz}{dw} = -\frac{U}{q} e^{i\theta} .$$

Hence

$$q = U/R , \ \theta = \beta + \pi ,$$

and (u, v) the velocity vector at $z(\zeta)$ is given by,

$$u = q \cos(\beta+\pi) = -q \cos\beta ,$$

$$v = q \sin(\beta+\pi) = -q \sin\beta .$$

The object now is to use the streamline and velocity information to set conditions on certain curves in the upper half of the complex z-plane. Specifically, we wish to know the pressure distribution along the segment $KLMN$ and the v velocity compoment on segment JK in Figure 7.

Assume that streamline RS passes through P on segment JK when $\zeta = \zeta_0 = \rho_0 e^{i\alpha}$ and through Q on segment LMN when $\zeta = \zeta_1 = \rho_1 e^{i\alpha}$. Using the previous notation, v_p, the v-velocity component at P is

$$v_p = -\frac{U}{R_0} \sin\beta_0 ,$$

where

$$\zeta_0 + (\zeta_0^2 - 1)^{1/2} = R_0 e^{i\beta_0} .$$

Furthermore, by Bernoulli's equation, p_Q, the pressure at Q is given by

$$p_Q = p_s + \frac{\delta U^2}{2}\left(1 - \frac{1}{R_1^2}\right) ,$$

where p_s = pressure at $S(\zeta = 0)$ and δ = fluid density are given constants, and R_1 is the magnitude of $\zeta_1 + (\zeta_1^2 - 1)^{1/2}$.

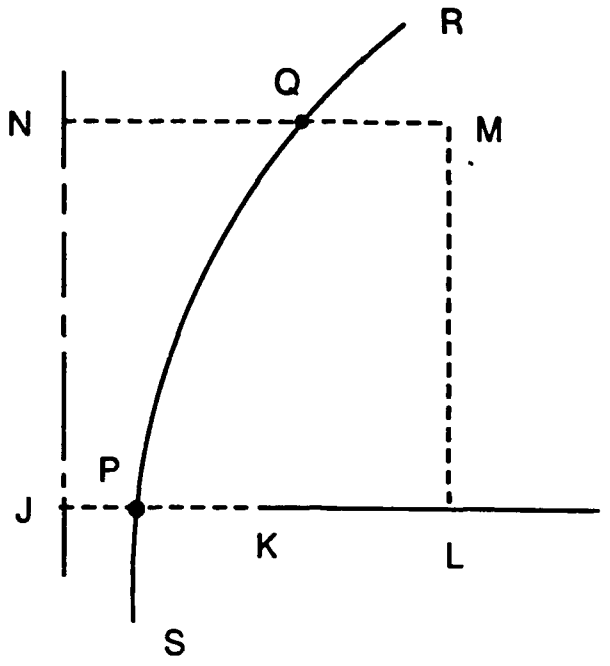

Figure 7. Boundary Curves.

Finally, we note that the above discussion applied to a jet issuing *from* a wall. The solution $\bar{u}$, $\bar{v}$, $\bar{p}$ corresponding to a jet *entering* the wall through the aperature is obtained from the solution u, v, p of the previous case by letting $\bar{u} = -u$, $\bar{v} = -v$, $\bar{p} = p$.

3. Numerical Experiments

The numerical procedure described in the previous section was applied to a plane jet problem with an aperature half width of .001 (see Figure 1). Streamlines of the anlaytic solution are shown in Figure 8. The derived pressure profiles along the far-field boundaries, and the velocity distribution at the mouth of the jet were then used to set the boundary conditions for a series of numerical simulations of this problem by means of the computer code ALGAE (Frey, Hall and Porsching [1987]). ALGAE produces finite difference solutions of various two dimensional fluid transport models under a wide variety of geometries and boundary conditions.

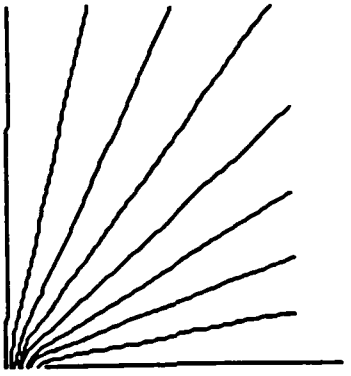

Figure 8. Analytic Solution Streamlines.

Figure 9 presents streamlines of a steady ALGAE numerical solution obtained on a 28×35 (nonuniform) grid utilizing an inviscid-flow model. Figure 10 shows the analogous information for a model incorporating a constant molecular viscosity of 0.02. Both solutions clearly reproduce the qualitative features of the analytic solution. The inviscid ALGAE numerical solution shows a tendency towards recirculation in the lower right-hand side of the flow region even though it is the inviscid model that gives rise to the analytic solution. This is due to a slight inaccuracy in the resolution of the jet's boundary layer where it meets the wall. Insufficient resolution of this boundary layer leads to numerical solutions that, as shown in Figure 11, are completely inaccurate. The viscous ALGAE numerical solution, on the other hand, shows no recirculation tendencies.

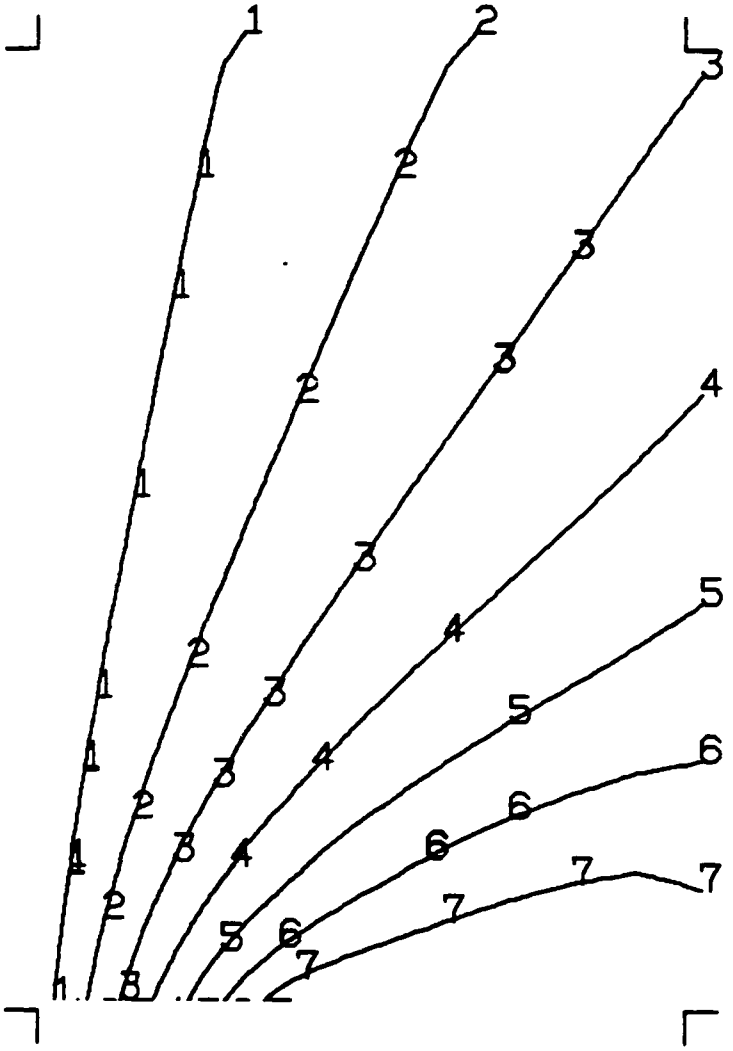

Figure 9. ALGAE Solution Streamlines, Inviscid Flow.

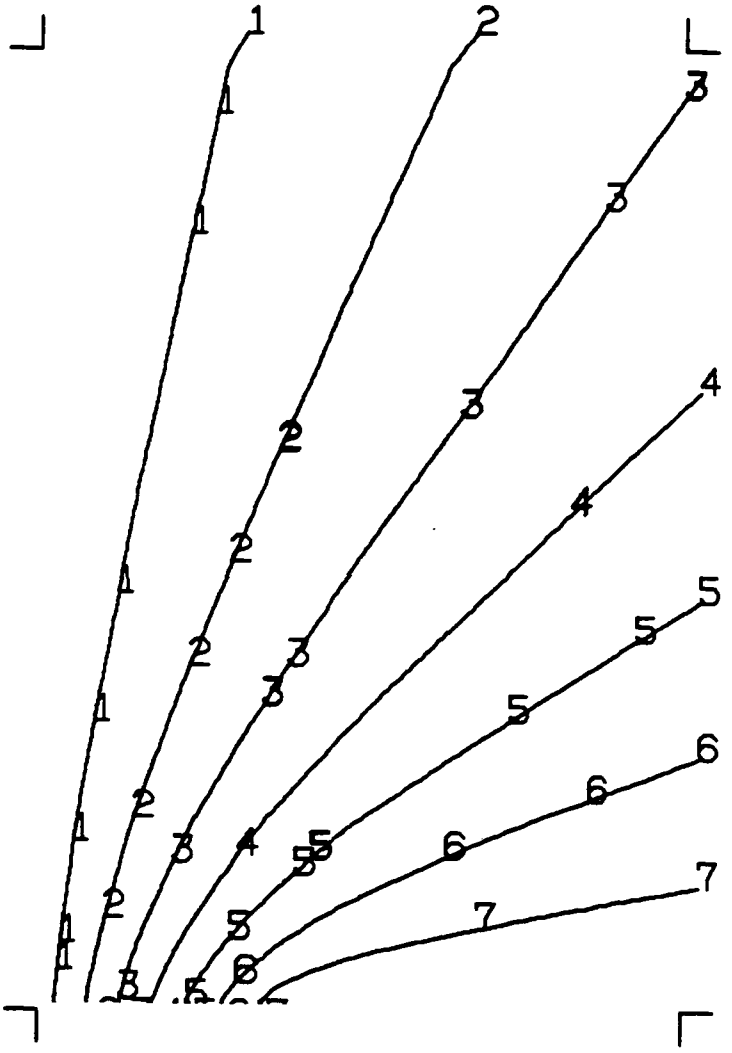

Figure 10. ALGAE Solution Streamlines, $\mu = .02$.

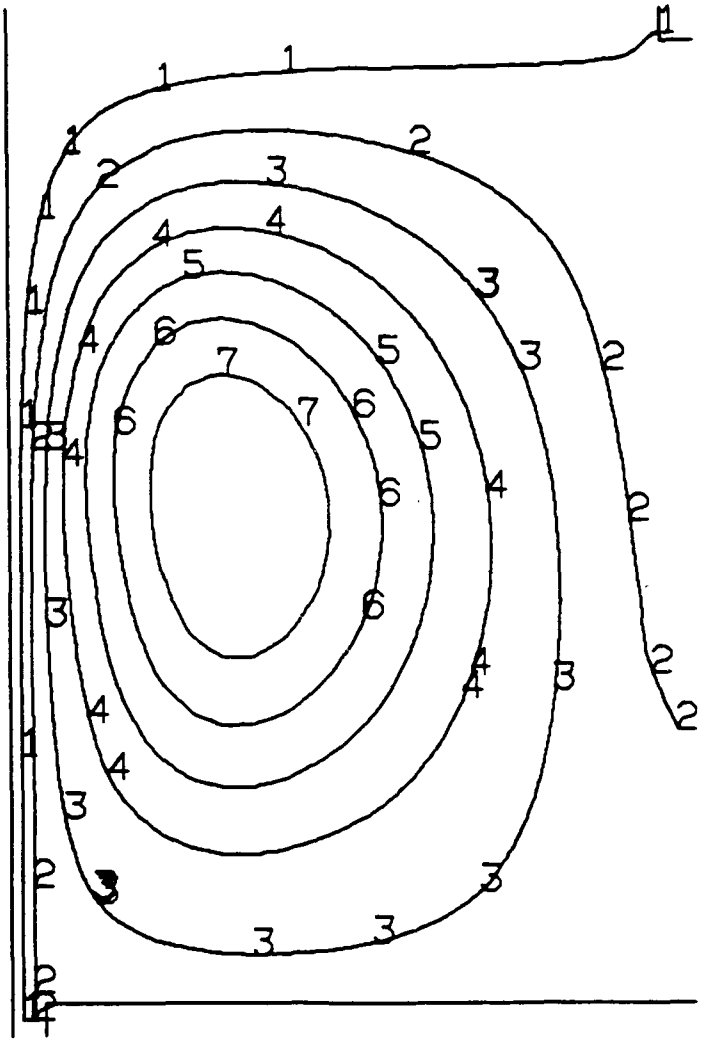

Figure 11. ALGAE Solution Streamlines, Insufficient Boundary Layer Resolution.

CHAPTER 3

DUAL VARIABLE SOLUTION OF THREE DIMENSIONAL, INCOMPRESSIBLE FLOW PROBLEMS

1. Introduction

The dual variable method (Amit, Hall and Porsching [1981], Dougall, Hall and Porsching [1982]) is a device to reduce the computational cost of solving the systems of (linear) equations that arise in many natural discretizations of fluid transport models. To date, the method has been applied to two dimensional transient problems. While the fundamental ideas of the method readily extend to three dimensions, implementations require the practical resolution of certain graph theoretic questions. In the remaining sections of this Chapter, we present the method in the context of the three dimensional Navier-Stokes equations, outline constructions and algorithms for its implementation, and give some preliminary numerical results and performance data.

2. The Dual Variable Method

We describe the method relative to a finite difference discretization of the well known three dimensional Navier-Stokes equations. We assume that the flow region is a rectangular parallelopiped, three of whose boundary planes form a portion of the first octant of a Cartesian coordinate system. We do not give the finite difference equations themselves since they are obvious generalizations of the two dimensional MAC equations presented in Amit, Hall and Porsching [1981] and Dougall, Hall and Porsching [1982].

To simplify the presentation in this section, we assume that the boundary conditions are homogeneous and the mesh spacings uniform. Then the resulting difference equations may be written in vector form as

$$AW = 0 , \tag{2.1}$$

$$QW = \Delta t \; A^T P + b . \tag{2.2}$$

Here $W \in R^L$ and $P \in R^N (L > N)$ are vectors of the unknown velocities and pressures. $A \in R^{N \times L}$ is the incidence matrix of a directed graph associated with the finite difference grid, $Q \in R^{L \times L}$ is the combined convection-diffusion operator, $b \in R^L$ is a vector of source terms, and Δt is the time step.

It can be shown that the rank of A is $N - 1$. Therefore, $\dim(\ker(A)) = L - N + 1$. Let $C \in R^{L \times (L-N+1)}$

have linearly independent columns and satisfy the orthogonality condition $AC = 0$. Any C satisfying these conditions is called a *fundamental matrix*. By (2.1), $W = C\gamma$ for some vector of "dual variables" $\gamma \in R^{L-N+1}$, and it follows from (2.2) that

$$C^T Q C \gamma = C^T b \ . \tag{2.3}$$

Note that whereas the size of (2.1), (2.2) is $L + N$, the size of (2.3) is $L - N + 1$. For three dimensional problems $L = O(3N)$, so that for large N (2.3) is about 1/2 the size of (2.1), (2.2).

The main algorithmic questions associated with (2.3) are the construction of C and the solution of (2.3) itself.

3. Construction of C; A Cycle Basis

By using the fact that A is the incidence matrix of a digraph, the construction of C is straightforwored in principle. Indeed, if the columns of C correspond to *any* set of $L - N + 1$ linearly independent cycles of the digraph, then C is a fundamental matrix (Berge and Ghouila-Houri [1965]). In the case of two dimensional problems (i.e. planar graphs), the choice of the *elementary cycles* leads to an especially sparse matrix C (no row has more than two nonzero entries). For three dimensional problems of the type considered here, Ye [1988] has given an analogous construction based on the four cycle stencils shown in Figure 1. Stencil (a) applys only on the lower horizontal "plane" of nodes in the graph, stencil (b) on the interior-horizontal planes, while the stencils of (c) and (d) apply respectively on the vertical "front" and "right" planes. These cycles are independent and a counting argument shows that there are exactly $L - N + 1$ of them.

4. Solution of Dual Variable Systems

At each time step it is necessary to solve the dual variable system (2.3). In the two dimensional case this was done directly by employing a "frontal" method. For three dimensional problems, the size of this system militates against such an approach [1] At the same time, empirical studies by Hageman [1975a, b] and Mesina [1988] demonstrate the efficiency of interative methods in the solution of large scale systems such as the one encountered here. Consequently, we consider the solution of (2.3) by means of an iteration.

1. If h is the uniform mesh spring, then the order of the coefficient matrix $C^T Q C$ is $O(2N) = O(2/h^3)$.

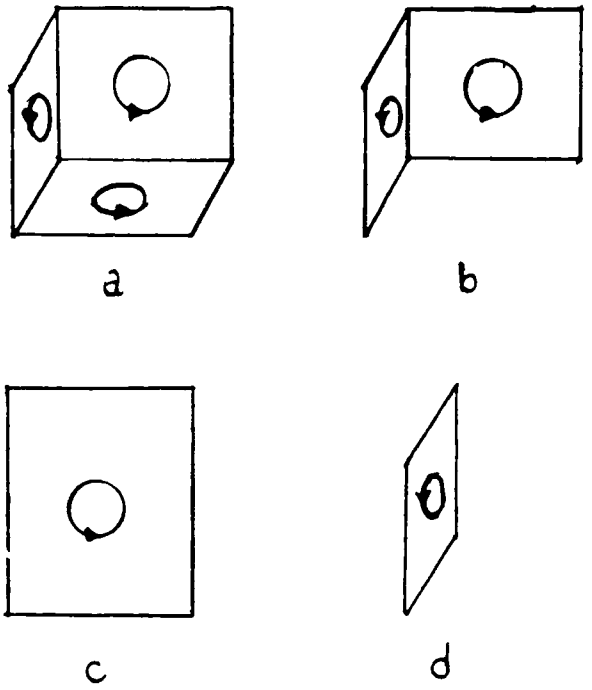

Figure 1. Cycle Stencils.

Classical iterative methods such as the (block) Gauss-Seidel and SOR methods are guaranteed to converge if the coefficient matrix is symmetric and positive definite (SPD). The same is true of projection methods such as gradient and (preconditioned) conjugate gradient methods. Unfortunately, the coefficient matrix C^TQC in (2.3) may fail to be SPD by virtue of a nonuniform mesh and/or convection effects. Thus, we devise a splitting of C^TQC whose diagonal block is SPD and is such that some of the nonsymmetric effects of the original matrix are incorporated into this block.

To describe this splitting, we let $Q = [q_{ij}]$ be any $J \times J$ matrix with a positive diagonal, $D = diag(q_{11}, \cdots, q_{JJ})$. (The matrix Q of (2.3) has this property). Now we split Q as

$$Q = D + E ,$$

where

$$E = [e_{ij}] , e_{ij} = \begin{cases} q_{ij} & i \neq j \\ 0 & i = j \end{cases}$$

Let $\theta > 0$ and consider the symmetric matrix,

$$\tilde{Q} = D + \theta(E + E^T) .$$

$\tilde{Q}$ will be strictly diagonally dominant if

$$q_{ii} > \sum_{j \neq i} \theta | q_{ij} + q_{ji} | , \ i = 1 , \ \cdots \ , J ,$$

i.e., if

$$\theta < r_i \equiv \frac{q_{ii}}{\sum_{j \neq i} | q_{ij} + q_{ji} |} , i = 1 , \ \cdots \ , J . \tag{4.1}$$

Thus, if θ satisfies (4.1), then $\tilde{Q}$ is a symmetric, strictly diagonally dominant matrix (and therefore SPD).

If Q is already symmetric and strictly diagonally dominant, then

$$q_{ii} > \sum_{j \neq i} | q_{ij} | , i = 1 , \ \cdots \ , J .$$

Therefore,

$$r_i = \frac{q_{ii}}{2 \sum_{j \neq i} | q_{ij} |} > \frac{1}{2} , i = 1 , \ \cdots \ , J . \tag{4.2}$$

In this case, the choice $\theta = 1/2$ satisfies (4.1) and in fact yields $\tilde{Q} = Q$. Guided by (4.1) and (4.2) we let

$$r = \min r_i .$$

Then we take

$$\theta = \begin{cases} \frac{1}{2} & \text{if } r > \frac{1}{2} \\ .9r & \text{if } r \leq \frac{1}{2} . \end{cases} \tag{4.3}$$

With this choice of θ we always obtain a SPD matrix $\tilde{Q}$. The corresponding SPD splitting for (2.3) is

$$C^T \tilde{Q} C \ \gamma = C^T (\tilde{Q} - Q) C \gamma + C^T b , \tag{4.4}$$

from which we deduce the (outer) iteration,

$$C^T \tilde{Q} C \gamma_k = C^T (\tilde{Q} - Q) C \gamma_{k-1} + C^T b . \tag{4.5}$$

System (4.5) is of the form $Au = f$ with

$$A = C^T \tilde{Q} C \ ,$$

$$u = \gamma_k \ ,$$

and

$$f = C^T(\tilde{Q} - Q)C\gamma_{k-1} + C^T b \ .$$

Note that if $\theta = 0$, then (4.5) reduces to the "Transformed Jacobi" method of Mesina [1988]. Note also that the factor .9 in (4.3) may be replaced by *any* positive quantity less than 1. Indeed, it can probably be replaced by 1 in practice. Its effect is to guarantee that $\tilde{Q}$ is strictly diagonally dominant (and hence SPD). But there are other conditions that imply positive definiteness. For example, if $\tilde{Q}$ is an irreducible matrix, and if $r_i \neq r_j$ for some $1 \leq i, j \leq J$, then for $\theta = r$, $\tilde{Q}$ is irreducibly diagonally dominant and so $C^T \tilde{Q} C$ is SPD.

Now we turn to the solution of the SPD system (4.5). In view of the above remarks, it suffices to consider the generic system

$$Au = f \ , \tag{4.6}$$

where A is an SPD matrix of order (say) N.

We apply the partial preconditioned conjugate gradient method (PPCG) to (4.6). The method can be described in algorithmic form as follows.

Initialization:

K = Number of PPCG iterations to the taken, $K \geq 1$.
n = Number of preconditioned conjugate gradient steps to be taken per iteration, $n \geq 1$.
u_0 = Initial approximation of u.
P = SPD splitting or preconditioning matrix.
ε = Convergence criterion, $\varepsilon > 0$.

1. $r_0 = f - Au_0$

2. If $r_0^T r_0 \leq \varepsilon$ then

   $u = u_0$
   Stop
   end if

3. For $k = 1, \cdots, K$

   $v_0 = u_{k-1}$
   For $j = 1, \cdots, n$
   Solve $Pz_{j-1} = r_{j-1}$ for z_{j-1}
   If $j = 1$, then

$\beta_1 = 0$
$p_1 = z_0$
else
$\beta_j = \dfrac{r_{j-1}^T z_{j-1}}{r_{j-2}^T z_{j-2}}$
$p_j = z_{j-1} + \beta_i p_{j-1}$
end if
$\alpha_j = \dfrac{r_{j-1}^T z_{j-1}}{p_j^T A p_j}$
$v_j = v_{j-1} + \alpha_j p_j$
$r_j = r_{j-1} - \alpha_j A p_j$
If $r_j^T r_j \leq \varepsilon$, then
$u = v_j$
Stop
end if
$u_k = v_n$

4. Print warning that convergence has not occurred.

5. $u = u_K$

6. Stop.

We remark that the PPCG algorithm reduces to the usual preconditioned conjugate gradient (PCG) algorithm if $K = 1$ and $n = N$.

Regarding the convergence rate of the PPCG method, it can be shown Luenberger [1973] that if the eigenvalues of the SPD matrix $P^{-1}A$ are

$$0 < \lambda_N \leq \lambda_{N-1} \leq \cdots \leq \lambda_n \leq \lambda_{n-1} \leq \cdots \leq \lambda_1 ,$$

and $e_k = u - u_k$, then

$$\|e_k\|_A \leq \left[\frac{\lambda_n - \lambda_N}{\lambda_n + \lambda_N}\right]^k \|e_0\|_A , \tag{4.7}$$

where $\|x\|_A \equiv (X^T A x)^{1/2}$. This proves the convergence of the algorithm for any choice of n. Moreover, if $n = N$, then $\|e_1\|_A = 0$, i.e. the algorithm converges in 1 step in the absence of roundoff. This is a well known feature of conjugate gradient algorithms. Since each iteration of of the PPCG algorithm incorporates n-steps of the PCG, we also have (Luenberger [1973]). the more familiar estimate,

$$\|e_k\|_A \leq 2\left[\frac{\sqrt{\lambda_1} - \sqrt{\lambda_N}}{\sqrt{\lambda_1} + \sqrt{\lambda_n}}\right]^n \|e_{k-1}\|_A . \tag{4.8}$$

Both estimates (4.7) and (4.8) indicate the desirability of choosing P such that $P^{-1}A$ has a narrow spectrum.

The PPCG algorithm may be implemented even when A is not SPD. However, this form of the algorithm can break down since it is now possible for $p_j^T A p_j$ to vanish. Also the estimates (4.7) and (4.8) no longer hold.

Each iteration of the PCG algorithm requires n system solves (for z_{j-1}) and n matrix-vector multiplications (for Ap_j). Storage for five vectors (z_{j-1}, p_j, Ap_j, r_j and v_j) is also needed. Clearly, the preconditioner P should be chosen so as to simplify the solution of $Pz_{j-1} = r_{j-1}$. For this reason, the choice $P = diag(a_{11}, \ldots, a_{NN})$ is often made. This gives rise to the partial Jacobi conjugate gradient (PJCG) method since it can be shown that the resulting algorithm is a polynomial accelerated version of the classical Jacobi method;

$$x_{k+1} = (I - P^{-1}A)x_k + P^{-1}f \ .$$

Another possible choice for P is

$$P = (B + \omega L)D^{-1}(D + \omega L)^T \ ,$$

where D and L are respectively the diagonal and lower triangle of A and $\omega \in (0,2)$ is a parameter. This yields the partial symmetric succesive over-relaxation conjugate gradient (PSSORCG) method. Note that solution of the system $Pz_{j-1} = r_{j-1}$ amounts to the solution of two triangular systems. The PJCG and PSSORCG methods can be implemented by restarting respectively the JCG and SSORCG subroutines of ITPACK software package (Kincaid et. al. [1981]).

5. Numerical Experiments

In this section we present some preliminary results from a computer code that utilizes the algorithmic approach described in the first four sections of this chapter. This code, R3IT, is under development at the University of Pittsburgh and runs on the CRAY XMP-48 at the Pittsburgh Supercomputing Center.

The test problems involve three dimensional driven cavity flows as described in Mansutti et. al. [1987]. The cavity is a cube two units on a side. No-slip boundary conditions are applied on the lid, floor and the two walls that are transverse to the motion of the lid. Depending on the simulation, either free or no-slip conditions hold on the two walls that align with the lid motion. The lid translates with a uniform unit velocity, and the Reynolds' number is 400.

Since the midplane between the two aligned walls is a plane of symmetry, it suffices to repalce this plane with a free-slip wall and simulate the flow in only one half of the cavity. Accordingly, a 10×10×5 uniform mesh is used to discretize this "half-problem". Note that when the free-slip condition is used on the remaining aligned wall, the problem becomes two-dimensional in the sense that there is no motion in the transverse direction.

Figure 2 shows floor-to-lid plots of the driven component of the velocity taken at the vertical centerline of the plane of symmetry. The 3-D simulation with a free-slip aligned wall reproduces a 2-D simulation obtained with the ALGAE code (Frey, Hall and Porsching [1987]). While there is general qualitative agreement between this solution and that of Mansutti et. al. [1987],, it shows considerably more dissipation than the latter. This is due to the well known numerical diffusion effect introduced by the use of upwind differences for the convection terms in R3IT. (See Chapter 1 for another illustration of this phenomenon.) When the no-slip condition is used on the aligned wall, the profile is even more attenuated in respone to the energy dissipation at that wall.

The 10×10×5 grid used in these simulations gives rise to a dual variable system (2.3) containing 805 unknowns. This is not large enough to exhibit the advantage of using an iterative method for its solution. In fact, a comparison of solution times shows that a direct solution of the system by LU decomposition is slightly faster than solution by the PPCG method of the previous section[1]. This is not surprising since other studies (see for example, Hageman [1975a] and Mesina [1988]) have also shown that direct methods are competitive with and sometimes faster than iterative methods for small problems. Such advantages disappear with increasing problem size.

[1] The direct solution time is 5.5 sec. per time step whereas the PPCG method solution time is 7.5 sec. per time step.

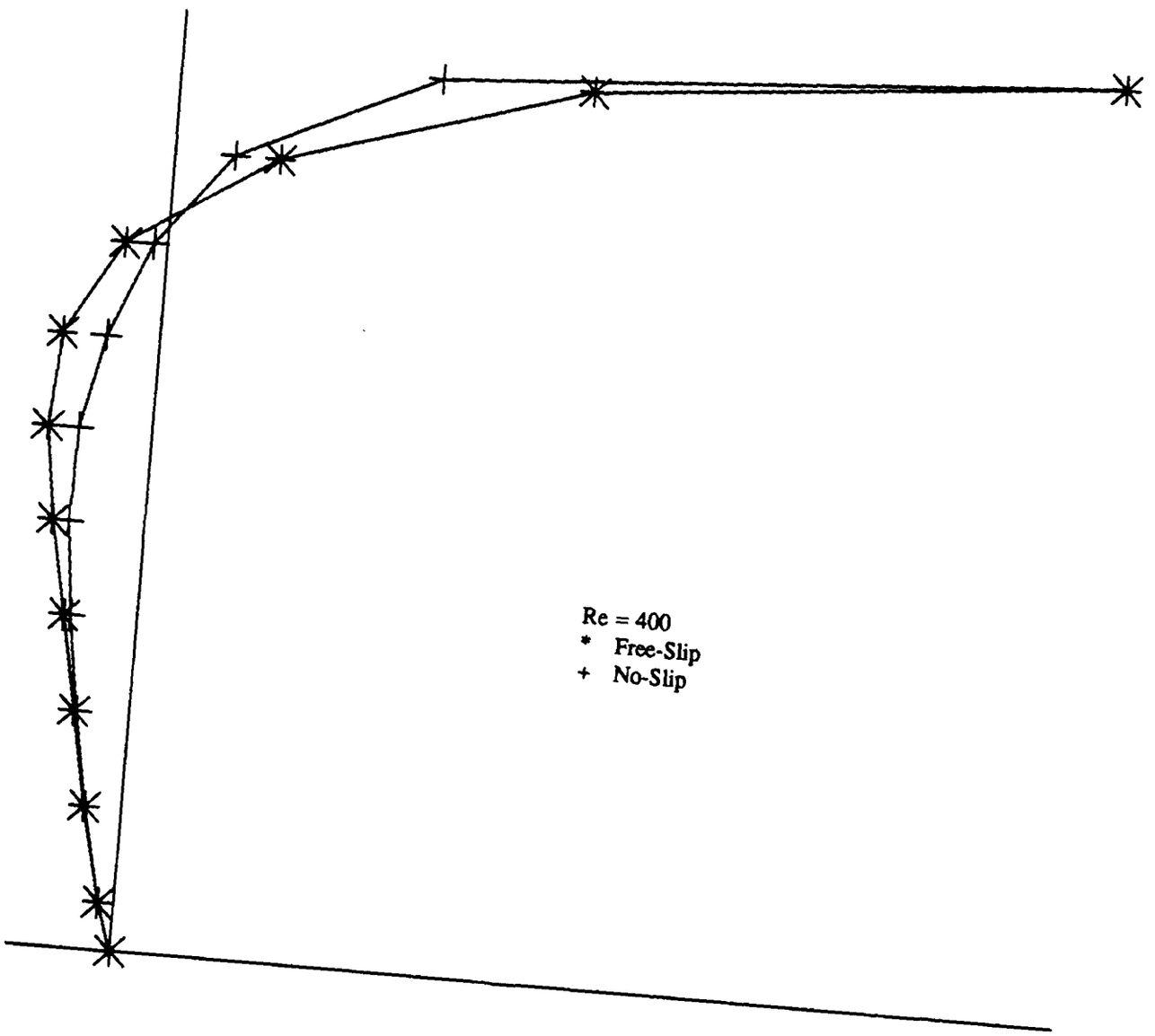

Figure 2. Vertical Profile of Driven Velocity Component.

References

Amit, R., Hall, C. A. and Porsching, T. A. [1981], "An Application of Network Theory to the Solution of Implicit Navier-Stokes Difference Equations," J. Comp. Physics *40*, pp. 183-201.

Berge, C. and Ghouila-Houri, A. [1965], *Programming, Games and Transportation Networks*, Methuen, 1965.

Book, D. L., Boris, J. P. and Hain, K. [1975], "Flux Corrected Transport II: Generalizations of the Method", J. Comp. Physics *18*, pp. 248-283.

Boris, J. P. and Book, D. L. [1973], "Flux Corrected Transport. I. SHASTA, A Fluid Transport Algorithm that Works", J. Comp. Physics *11*, pp. 38-69.

Boris, J. P. and Book. D. L. [1976], "Flux Corrected Transport. III. Minimal-Error FCT Algorithms", J. Comp. Physics *20*, pp. 397-431.

Dougall, R. S., Hall, C. A. and Porsching, T. A. [1982], *DUVAL: A Computer Program for the Numerical Solution of Two-Dimensional, Two-Phase Flow Problems*, Volumes 1-3, Electric Power Research Institute Report NP-2099, Palo Alto, CA.

Frey, A., Hall, C. A. and Porsching, T. A. [1987], "Numerical Simulation of Confined Unsteady Aerodynamical Flows", Int. J. Num. Meth. Engr. *24*, pp. 1233-1250.

Hageman, L. A. [1975a], *The Solution of Linear Equations Resulting from Finite Element Discretizations of Multi-Dimensional Boundary Value Problems*, WAPD-TM-1209, Bettis Atomic Power Laboratory, West Mifflin, PA.

Hageman, L. A. [1975b], *Computational Aspects in the Numerical Solution of Partial Differential Equations*, WAPD-T-2624, Bettis Atomic Power Laboratory, West Mifflin, PA.

Harten, A. [1983], "High Resolution Schemes for Hyperbolic Conservation Laws", J. Comp. Physics *49*, pp. 357-393.

Harten, A. [1984], "On a Class of High Resolution Total-Variation-Stable Finite-Difference Schemes", SIAM J. Numer. Anal. *21*, pp. 1-23.

Harten, A. and Zwas, G. [1972], "Self-adjusting Hybrid Schemes for Shock Computation", J. Comp. Physics *6*, pp. 568-583.

Helmholtz, H. [1868], Phil. Mag. (November).

Kincaid, D., Grimes, R., Respess, J. and Young, D. [1981], "ITPACK 2B: A FORTRAN Implementation of Adaptive Accelerated Iterative Methods for Solving Large Sparse Linear Systems", CNA-173, Center for Numerical Analysis, Univ. of Texas.

Ladyzhenskaya, O. A. [1985], *The Boundary Value Problems of Mathematical Physics*, Springer Verlag, 1985.

Luenberger, D. G. [1973], *Introduction to Linear and Nonlinear Programming*, Addison-Wesley, 1973.

Mansutti, D., Bulgarelli, U., Piva, R. and Graziani, G. [1987], "A Discrete Vector Potential Method for Unsteady 3-D Navier-Stokes Equations," Int. Conf. on Numer. Meth. in Fluid Mechanics, Beijing (1986), *Lecture Notes in Physics*, Springer Verlag, 1987.

Mesina, G. [1988], "Iterative Solutions to the Navier-Stokes Difference Equations", Ph.D. Dissertation, University of Pittsburgh, 1988.

Woodward, P. and Colella, P. [1984], "The Numerical Simulation of Two-Dimensional Fluid Flow with Strong Shocks", J. Comp. Physics *54*, pp. 115-173.

Ye, X. [1988], "Construction of Divergence-Free Spaces for Incompressible Navier-Stokes Equations", Ph.D. Dissertation, University of Pittsburgh (in preparation).

Zalesak, S. T. [1979], "Fully Multidimensional Flux-Corrected Transport Algorithms for Fluids", J. Comp. Physics *31*, pp. 335-362.